SABA Publishing

Journal of Fractional Calculus and Nonlinear Systems
jfcns.sabapub.com
ISSN : 2709-9547

J Frac Calc & Nonlinear Sys
(2026)7(1) : 28-57
doi:10.48185/jfcns.v7i1.1816

Analysis of Stability in Rulkov Neural Networks with Fractional Orders and Asymmetric Memristor Synapses

LEILA EFTEKHARI[a,*], MOEIN KHALIGHI[b], SAEID ABBASBANDY[a]

[a] Department of Applied Mathematics, Imam Khomeini International University, Qazvin, Iran
[b] Department of Computing, University of Turku; 20500 Turku, Finland

• *Received: 21 September 2025* • *Accepted: 05 March 2026* • *Published Online: 30 6 2026*

Abstract

Fractional-order models effectively capture memory and hereditary effects in neural and nonlinear dynamical systems. Memristors are ideal components for modeling synaptic connections due to their ability to emulate plasticity and memory effects. Discrete models of memristor-coupled neurons simplify computations and enable efficient analysis of large-scale networks. Despite their potential, discrete fractional-order memristor-coupled models have been less explored. To address this, we propose two novel discrete fractional-order neural systems. The first system is a two-neuron motif coupled via dual memristors, while the second extends this configuration to a ring-shaped network of similar subnetworks. A new theorem on the stability of discrete fractional-order systems is established, defining stability regions for both models. Numerical simulations illustrate the theoretical results and investigate how the fractional order, asymmetric memristive coupling, and other model and network parameters jointly influence the dynamics and stability of discrete-time neurons.

Keywords: Discrete fractional calculus, Fractional order neural networks, Memristor-coupled neurons, Stability analysis, Ring neural network

1. Introduction

Artificial neural networks (ANNs) and mathematical models are widely used to simulate the brain's complex activities, providing deeper insights into neural mechanisms [1]. Neurons do not function in isolation; their interactions are crucial for neural processing. Modeling these neuronal connections using physical devices is pivotal in network modeling. Due to their nonlinear behavior, nanoscale dimensions, and memory features, memristors are considered artificial synapses and are widely used in chaotic circuits and neural networks [2, 3]. Coupling discrete dual memristors instead of individual ones in neural maps allows for better exploration of complex neuronal behaviors [4].

Neuronal models are typically categorized into continuous-time models and discrete-time models [5]. While continuous neural models have been extensively studied, discrete

*Corresponding author: leila.eftekhari32@gmail.com

models can more effectively simulate random and paroxysmal intracellular ion dynamics. Discrete-time models are significant for their computational advantages and suitability for digital hardware implementations, aligning well with the integration of memristors as artificial synapses. Several neuron models are formulated as discrete-time dynamical systems, including the Izhikevich, Rulkov, Courbage-Nekorkin-Vdovin, and Chialvo models [25, 7, 8].

Many well-known models describing neuronal dynamics are based on ordinary differential equations, such as the Morris–Lecar and FitzHugh–Nagumo models [9, 10]. However, classical integer-order models may fail to fully capture memory and hereditary effects observed in real biological systems. Fractional differential equations and differences have therefore attracted significant attention due to their inherent nonlocal properties, which allow them to reflect the history of a process more accurately. Moreover, fractional calculus has opened new avenues in diverse fields, including biology, ecology, electric power systems, and neural networks [11, 12, 13, 14, 15, 16]. The existence and uniqueness of solutions for fractional-order systems under various boundary conditions have been well studied, including Ψ-fractional hybrid systems with periodic [17], implicit fractional differential equations with anti-periodic [18], and nonlinear fractional integro-differential equations [19].

Recent advances, including fractional quantum calculus [20], control-theoretic approaches for fractional-order systems [21], and stability analysis of discrete fractional neural networks [22], have further enriched the mathematical framework for analyzing nonlinear dynamics and stability. In discrete-time settings, the nabla fractional difference offers advantages over the delta operator by avoiding domain-shift issues and enabling richer dynamical behaviors [6]. Incorporating fractional-order dynamics into memristor-coupled neural models therefore enables effective modeling of long-term memory effects, complex firing patterns, and non-Markovian neuronal behavior [26, 27].

Despite these advancements, existing discrete memristive neural networks mostly focus on single-memristor coupling or simplified linear interactions, which fail to capture the full spectrum of biological neuronal dynamics [3]. Coupling neurons via dual memristors can generate complex behaviors like extreme transient dynamics, better reflecting real neuronal operations [9]. However, incorporating fractional-order discrete calculus, particularly with the nabla operator, into such dual memristor-coupled networks remains underexplored, Table 1.

To address this gap, we propose a novel fractional-order discrete memristor-coupled neural network. We construct a Fractional Discrete Memristor-Coupled Rulkov Neuron (FDMCRN) map by coupling two Rulkov neurons via dual flux-controlled memristors, employing the Caputo nabla fractional difference to model the fractional dynamics. We subsequently expand the model into a ring network configuration of FDMCRN maps, providing theoretical foundations for stability analysis of the ring structure, crucial for understanding long-term neural network behavior. Finally, we numerically investigate the stability criteria for both systems and evaluate how initial conditions influence the dynamics of the FDMCRN model.

Table 1: Comparison of recent discrete fractional-order neuron models with memristive coupling and stability analysis (2021–2025)

Reference (Year)	Fractional Operator	Neuron Model	Memristor Synapse	Topology	Stability Analysis
Almatroud (2021) [24]	Caputo Delta	Generic Neuron	×	Small Network	Numerical
Lu et al. (2022) [29]	Caputo Delta	Rulkov	Single Memristor	Single Neuron	Numerical
Hiouala et al. (2022) [23]	Caputo Nabla	Generic Neuron	×	Network	Analytical + Numerical
Vivekanandhan et al. (2023) [5]	Caputo Delta	Rulkov	×	Single Neuron	Analytical + Numerical
Ghasemi et al. (2024) [22]	Caputo Delta	Rulkov	Single Memristor	Two Neuron	Analytical + Numerical
This Work	**Caputo Nabla Fractional**	**Rulkov**	**Dual Memristor**	**Ring Network**	**Analytical + Numerical**

2. Materials and Methods

The following definitions introduce the necessary fractional operators used throughout this work.

Remark 2.1. In this article, we consistently work within the framework of a discrete time scale, $\mathbb{N}_b = \{b, b+1, b+2, ...\}$, where $b \in \mathbb{R}$ is fixed. For any function $f : \mathbb{N}_b \to \mathbb{R}$, the backward difference, also known as the nabla operator, is defined as follows, $\nabla f(n) = f(n) - f(n-1)$ for $n \in \mathbb{N}_{b+1}$.

Definition 2.2. [31] For any real numbers τ and n, the τ rising function is defined by

$$n^{\overline{\tau}} = \frac{\Gamma(n+\tau)}{\Gamma(n)}, n \in \mathbb{R} \setminus \{\dots, -2, -1, 0\}, 0^{\overline{\tau}} = 0, \tag{2.1}$$

Definition 2.3. [30] (Nabla fractional sum) Suppose $f : \mathbb{N}_0 \to \mathbb{R}$ and $\alpha \in (0,1)$ be provided, The nabla fractional sum of order α for the function f is expressed as follows

$$\nabla^{-\alpha} f(n) = \frac{1}{\Gamma(\alpha)} \sum_{s=1}^{n} (n - \rho(s))^{\overline{\alpha-1}}, \tag{2.2}$$

where $\rho(s) = s - 1$, $n \in \mathbb{N}_0$.

Definition 2.4. [31] Let $f : \mathbb{N}_0 \to \mathbb{R}$ and $\alpha \in (0,1)$, the Caputo-type fractional nabla difference of order α for f is

$${}_0^C\nabla^{\alpha} f(n) := ({}_0\nabla^{-(1-\alpha)}\nabla f)(n) = \frac{1}{\Gamma(1-\alpha)} \sum_{s=a+1}^{n} (n - s + 1)^{\overline{-\alpha}} (\nabla f)(s), \tag{2.3}$$

for $\alpha = 0$ we get $\nabla_0^0 f(n) = f(n)$ and $n \in \mathbb{N}_1$.

2.1. Mathematical representations

FDMCRN Framework. Using the definition (2.2) and based on the mathematical expression of the discrete-time memristor [28, 29], the difference equation of the Rulkov

neuron map can be derived the following form

$$\begin{cases} {}_0^C\nabla^\alpha x_{1,n+1} = \frac{a}{1+x_{1,n}^2} + y_{1,n} + k\varphi_{1,n}(x_{1,n} - x_{2,n}) - x_{1,n}, \\ {}_0^C\nabla^\alpha y_{1,n+1} = -\eta(x_{1,n} - \sigma) + k\varphi_{2,n}(y_{1,n} - y_{2,n}), \\ {}_0^C\nabla^\alpha x_{2,n+1} = \frac{a}{1+x_{2,n}^2} + y_{2,n} - k\varphi_{1,n}(x_{1,n} - x_{2,n}) - x_{2,n}, \\ {}_0^C\nabla^\alpha y_{2,n+1} = -\eta(x_{2,n} - \sigma) - k\varphi_{2,n}(y_{1,n} - y_{2,n}), \\ {}_0^C\nabla^\alpha \varphi_{1,n+1} = x_{1,n} - x_{2,n}, \\ {}_0^C\nabla^\alpha \varphi_{2,n+1} = y_{1,n} - y_{2,n}, \end{cases} \tag{2.4}$$

where n denotes the iterations and k is the coupling strength between the pair of neurons. The variables $x_{1,n}, x_{2,n}$ represent the neurons' membrane potentials influenced by a nonlinear map parameter a. The recovery variables $y_{1,n}, y_{2,n}$ are influenced by parameters $0 < \eta < 1$ and σ, which is an external DC to neurons. Additionally, $\varphi_{1,n}$ and $\varphi_{2,n}$ denote the fluxes of the two neurons at iteration n. The schematic connection pattern of the FDMCRN, consisting of two neurons with two coupling memristors, is depicted in Fig. 1.

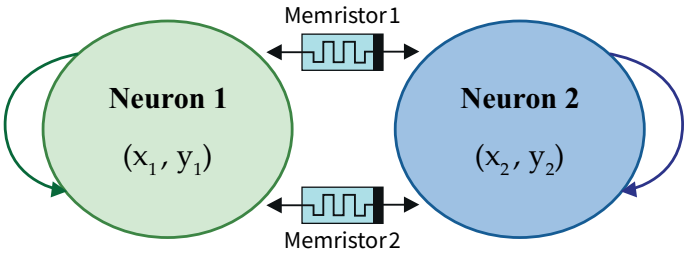

Figure 1: Schematic diagram of the FDMCRN model model showing two neurons coupled via dual memristors.

FDMCRN Framework With Ring Configuration. We extend the FDMCRN model (2.4) from two neurons to N units by implementing a ring-network structure, as depicted in Fig. 2. In this configuration, the N units are coupled, and the membrane potentials x_{1i} evolve according to the following equations:

$$\begin{cases} {}_0^C\nabla^\alpha x_{1i,n+1} = \frac{a}{1+x_{1i,n}^2} + y_{1i,n} + k\varphi_{1i,n}(x_{1i,n} - x_{2i,n}) - x_{1i,n} + \frac{D}{2P}\sum_{j=i-P}^{i+P}(x_{1j} - x_{1i}), \\ {}_0^C\nabla^\alpha y_{1i,n+1} = -\eta(x_{1i,n} - \sigma) + k\varphi_{2i,n}(y_{1i,n} - y_{2i,n}), \\ {}_0^C\nabla^\alpha x_{2i,n+1} = \frac{a}{1+x_{2i,n}^2} + y_{2i,n} - k\varphi_{1i,n}(x_{1i,n} - x_{2i,n}) - x_{2i,n}, \\ {}_0^C\nabla^\alpha y_{2i,n+1} = -\eta(x_{2i,n} - \sigma) - k\varphi_{2i,n}(y_{1i,n} - y_{2i,n}), \\ {}_0^C\nabla^\alpha \varphi_{1i,n+1} = x_{1i,n} - x_{2i,n}, \\ {}_0^C\nabla^\alpha \varphi_{2i,n+1} = y_{1i,n} - y_{2i,n}. \end{cases} \tag{2.5}$$

where $i = 1$ to N and the state variables of the i^{th} unit are represented as $(x_{1i}, y_{1i}, x_{2i}, y_{2i}, \varphi_{1i}, \varphi_{2i})$. The memristor synapses couple symmetrically to the 2P nearest neighbors, every unit engages with P neighboring units to its left and right. Here, P denotes the set of indices corresponding to the neighbors of the i^{th} unit and D represents the connection strength between the N units.

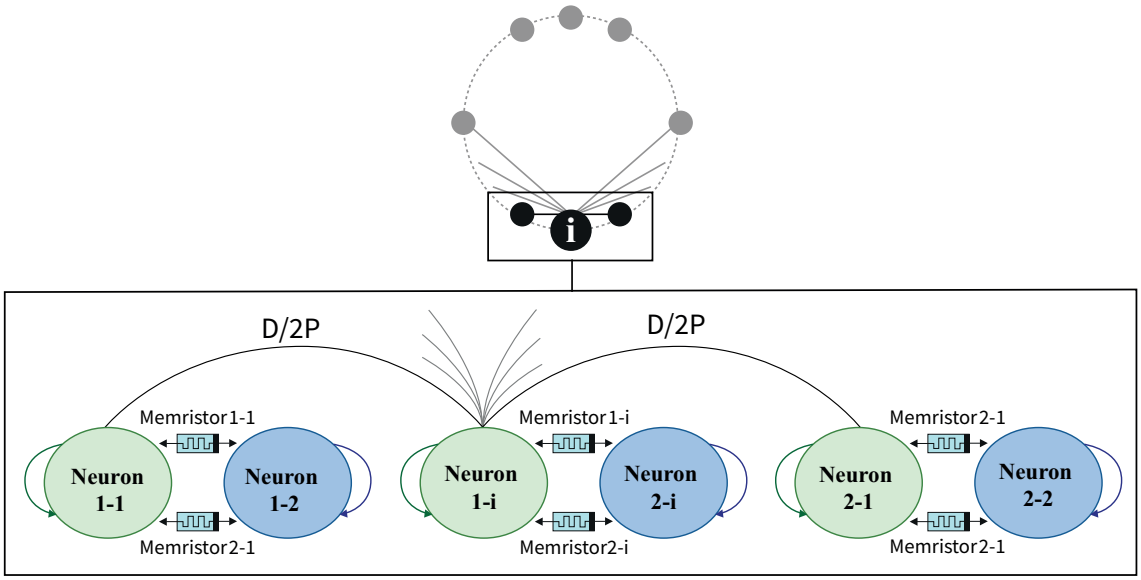

Figure 2: Schematic of the i-th unit in the ring network comprising the FDMCRN model

2.2. Analysis of the model

This section explores whether solutions exist and if they are unique, along with establishing the stability conditions for models (2.4) and (2.5). To achieve this, certain fundamental definitions are necessary; therefore, each subsection begins with this essential evidence.

2.2.1. Existence and Uniqueness of Solutions

Definition 2.5. A **circulant matrix** is a structured square matrix where each row is defined as

$$C = \mathrm{circ}(b_0, b_1, ..., b_{N-1}) = \begin{bmatrix} c_0 & c_1 & c_2 & c_3 & \ddots & c_{N-2} & c_{N-1} \\ c_{N-1} & c_0 & c_1 & c_2 & \ddots & c_{N-3} & c_{N-2} \\ c_{N-2} & c_0 & c_1 & c_2 & \ddots & c_{N-4} & c_{N-3} \\ \ddots & \ddots & \ddots & \ddots & \ddots & \ddots & \ddots \\ c_2 & c_3 & c_4 & c_5 & \ddots & c_0 & c_1 \\ c_1 & c_2 & c_3 & c_4 & \ddots & c_{N-1} & c_0 \end{bmatrix}_{N\times N}.$$

A **block circulant matrix** extends the concept of a circulant matrix by having each block as an individual circulant matrix.

$$C = \text{bcirc}(C_0, C_1, ..., C_{N-1}) = \begin{bmatrix} C_0 & C_1 & C_2 & C_3 & \ddots & C_{N-2} & C_{N-1} \\ C_{N-1} & C_0 & C_1 & C_2 & \ddots & C_{N-3} & C_{N-2} \\ C_{N-2} & C_0 & C_1 & C_2 & \ddots & C_{N-4} & C_{N-3} \\ \ddots & \ddots & \ddots & \ddots & \ddots & \ddots & \ddots \\ C_2 & C_3 & C_4 & C_5 & \ddots & C_0 & C_1 \\ C_1 & C_2 & C_3 & C_4 & \ddots & C_{N-1} & C_0 \end{bmatrix}_{N\times N}.$$

The C_i matrices for $i = 0$ to $N-1$ are block-formatted matrices [15].

Theorem 2.6. *Suppose that* $\Omega = \{(x_1, y_1, x_2, y_2, \varphi_1, \varphi_2) \in R^6$, $S = \Omega \times \mathbb{N}_1$ *where* $n < \infty$ *and* $\max\{\|x_i\|, \|y_i\|, \|\varphi_i\|\} \leqslant \zeta\}$, *i=1,2. For any initial conditions* $X_0 = (x_{1,0}, y_{1,0}, x_{2,0}, y_{2,0}, \varphi_{1,0}, \varphi_{2,0}) \in \Omega$, *for every n, all the solutions* $X_n \in S$ *of system (2.4) are unique.*

Proof. The proof is based on establishing the local Lipschitz continuity of the system mapping. To this end, the right-hand side of system (2.4) is decomposed into three parts: a bounded nonlinear term, a linear term, and a memristive coupling term. Each component is shown to satisfy a Lipschitz-type estimate on the set S.
Specifically, assume $\mathbb{F}(X_n) = (\mathbb{F}_1(X_n), \mathbb{F}_2(X_n), \mathbb{F}_3(X_n), \mathbb{F}_4(X_n), \mathbb{F}_5(X_n), \mathbb{F}_6(X_n))^T$ represents a mapping function with the $\|.\|$ norm, ensuring that

$$\begin{aligned}
\mathbb{F}_1(X_n) &= \frac{a}{1+x_{1,n}^2} + y_{1,n} + k\varphi_{1,n}(x_{1,n} - x_{2,n}) - x_{1,n}, \\
\mathbb{F}_2(X_n) &= -\eta(x_{1,n} - \sigma) + k\varphi_{2,n}(y_{1,n} - y_{2,n}), \\
\mathbb{F}_3(X_n) &= \frac{a}{1+x_{2,n}^2} + y_{2,n} - k\varphi_{1,n}(x_{1,n} - x_{2,n}) - x_{2,n}, \\
\mathbb{F}_4(X_n) &= -\eta(x_{2,n} - \sigma) - k\varphi_{2,n}(y_{1,n} - y_{2,n}), \\
\mathbb{F}_5(X_n) &= x_{1,n} - x_{2,n}, \\
\mathbb{F}_6(X_n) &= y_{1,n} - y_{2,n},
\end{aligned}$$

where $X_n = (x_{1,n}, y_{1,n}, x_{2,n}, y_{2,n}, \varphi_{1,n}, \varphi_{2,n})^T$. Consequently, the mapping function can be expressed in the form below

$$\mathbb{F}(X_n) = \Psi(X_n) + AX_n + k\Phi X_n,$$

such that

$$\Psi(X_n) = \begin{bmatrix} \frac{a}{1+x_{1,n}^2} \\ \eta\sigma \\ \frac{a}{1+x_{2,n}^2} \\ \eta\sigma \\ 0 \\ 0 \end{bmatrix}, A = \begin{bmatrix} -1 & 1 & 0 & 0 & 0 & 0 \\ -\eta & 0 & 0 & 0 & 0 & 0 \\ 0 & 0 & -1 & 1 & 0 & 0 \\ 0 & 0 & -\eta & 0 & 0 & 0 \\ 1 & 0 & -1 & 0 & 0 & 0 \\ 0 & 1 & 0 & -1 & 0 & 0 \end{bmatrix},$$

$$\Phi = \begin{bmatrix} \varphi_{1,n} & 0 & -\varphi_{1,n} & 0 & 0 & 0 \\ 0 & \varphi_{2,n} & 0 & -\varphi_{2,n} & 0 & 0 \\ -\varphi_{1,n} & 0 & \varphi_{1,n} & 0 & 0 & 0 \\ 0 & -\varphi_{2,n} & 0 & \varphi_{2,n} & 0 & 0 \\ 0 & 0 & 0 & 0 & 0 & 0 \\ 0 & 0 & 0 & 0 & 0 & 0 \end{bmatrix}, X_n = \begin{bmatrix} x_{1,n} \\ y_{1,n} \\ x_{2,n} \\ y_{2,n} \\ \varphi_{1,n} \\ \varphi_{2,n} \end{bmatrix}.$$

Since $\Psi(X)$ consists of smooth rational functions and constant terms, it is continuous and consequently satisfies the Lipschitz condition [32], i.e:

$$\forall X, \bar{X} \in S,\ \exists \zeta_1 \geqslant 0 \quad s.t\ \ ||(\Psi(x) - \Psi(\bar{x})|| \leqslant \zeta_1 ||x - \bar{x}|| \tag{2.6}$$

We now prove that the system (2.4) satisfies the locally Lipschitz condition:

$$\forall X, \bar{X} \in S,\ \exists L \geqslant 0 \quad s.t\ \ ||\mathbb{F}(X) - \mathbb{F}(\bar{X})|| \leqslant L||X - \bar{X}||$$

Where

$$X = \left(x_{1,n_1}, y_{1,n_1}, x_{2,n_1}, y_{2,n_1}, \phi_{1,n_1}, \phi_{2,n_1}\right), \overline{X} = \left(\overline{x}_{1,n_2}, \overline{y}_{1,n_2}, \overline{x}_{2,n_2}, \overline{y}_{2,n_2}, \overline{\phi}_{1,n_2}, \overline{\phi}_{2,n_2}\right),$$

$$\begin{aligned} ||\mathbb{F}(x) - \mathbb{F}(\bar{x})|| &= ||(\Psi(x) - \Psi(\bar{x}) + A(x - \bar{x}) + k(\Phi x - \bar{\Phi}\bar{x})|| \\ &\leqslant ||(\Psi(x) - \Psi(\bar{x})|| + ||A||\ ||x - \bar{x}|| + ||k\Phi||\ ||x - \bar{x}|| \\ &\leqslant (\zeta_1 + ||A|| + k\ \zeta)\ ||x - \bar{x}|| \\ &= L||x - \bar{x}||,\ L = \zeta_1 + ||A|| + k\ \zeta. \end{aligned}$$

Thus, the solution to the model (2.4) is unique within S. □

Theorem 2.7. *Suppose that* $\Omega = \{(x_1, y_1, x_2, y_2, \phi_1, \phi_2) \in \mathbb{R}^{N\times 6}$, *s.t* $x_1 = [x_{1i,n}]_{N\times 1}$, $y_1 = [y_{1i,n}]_{N\times 1}, x_2 = [x_{2i,n}]_{N\times 1}, y_2 = [y_{2i,n}]_{N\times 1}$, $\phi_1 = [\varphi_{1i,n}]_{N\times 1}$, $\phi_2 = [\varphi_{2i,n}]_{N\times 1}$, $\Lambda = [\lambda_i]_{N\times 1}$, $\max\{||x_1||, ||y_1||, ||x_2||, ||y_2||, ||\phi_1||, ||\phi_2||\} \leqslant \Lambda\}_{|i=1,2,\ldots,N}$ *and* $S = \Omega \times \mathbb{N}_1$. *For any chosen initial conditions* $(x_{1,0}, y_{1,0}, x_{2,0}, y_{2,0}, \phi_{1,0}, \phi_{2,0}) \in \Omega$, *all the solutions* $X_n \in S$ *of model (2.5) are unique.*

Proof. The proof follows the same strategy as in the low-dimensional model (2.4) and is based on establishing the local Lipschitz continuity of the network mapping. To this end, the right-hand side of model (2.5) is decomposed into a bounded nonlinear term, a linear term represented by a block circulant matrix, and a memristive coupling term. Each

component is shown to satisfy a Lipschitz-type estimate on the bounded set S. Suppose

$$X_n = (X_{1,n}, Y_{1,n}, X_{2,n}, Y_{2,n}, \phi_{1,n}, \phi_{2,n})^T$$

$$\mathbb{F}(X_n) = (\mathbb{F}_1(X_n), \mathbb{F}_2(X_n), \mathbb{F}_3(X_n), \mathbb{F}_4(X_n), \mathbb{F}_5(X_n), \mathbb{F}_6(X_n))^T$$

act as a function that maps multiple variables while utilizing the $\|.\|$ norm in such a way that

$$\begin{aligned}
\mathbb{F}_1(X_n) &= \frac{a}{1+x_{1i,n}^2} + y_{1i,n} + k\varphi_{1i,n}(x_{1i,n} - x_{2i,n}) - x_{1i,n} + \frac{D}{2P}\sum_{j=i-P}^{i+P}(x_{1j,n} - x_{1i,n}),\\
\mathbb{F}_2(X_n) &= -\eta(x_{1i,n} - \sigma) + k\varphi_{2i,n}(y_{1i,n} - y_{2i,n}),\\
\mathbb{F}_3(X_n) &= \frac{a}{1+x_{2i,n}^2} + y_{2i,n} - k\varphi_{1i,n}(x_{1i,n} - x_{2i,n}) - x_{2i,n},\\
\mathbb{F}_4(X_n) &= -\eta(x_{2i,n} - \sigma) - k\varphi_{2i,n}(y_{1i,n} - y_{2i,n}),\\
\mathbb{F}_5(X_n) &= x_{1i,n} - x_{2i,n},\\
\mathbb{F}_6(X_n) &= y_{1i,n} - y_{2i,n},
\end{aligned}$$

It can be written as follows

$$\mathbb{F}(X_n) = \Psi(X_n) + AX_n + k\widetilde{\Phi}X_n \quad \widetilde{\Phi} = \mathrm{bcirc}(\Phi, 0, .., 0)_{1\times N},$$

$$\Psi(X_n) = \mathrm{bcirc}(\phi(X_n), \phi(X_n), .., \phi(X_n))_{1\times N}$$

Matrix $A \in \mathbb{R}^{N\times N}$ is a block circulant matrix constructed from the blocks $A_0, A_1, ..., A_1$, such that $A_0, A_1 \in \mathbb{R}^{6\times 6}$,

$$A_0 = \begin{bmatrix} -1-\frac{D}{P} & 1 & 0 & 0 & 0 & 0\\ -\eta & 0 & 0 & 0 & 0 & 0\\ 0 & 0 & -1 & 1 & 0 & 0\\ 0 & 0 & -\eta & 0 & 0 & 0\\ 1 & 0 & -1 & 0 & 0 & 0\\ 0 & 1 & 0 & -1 & 0 & 0 \end{bmatrix}, A_1 = \begin{bmatrix} \frac{D}{2P} & 0 & 0 & 0 & 0 & 0\\ 0 & 0 & 0 & 0 & 0 & 0\\ 0 & 0 & 0 & 0 & 0 & 0\\ 0 & 0 & 0 & 0 & 0 & 0\\ 0 & 0 & 0 & 0 & 0 & 0\\ 0 & 0 & 0 & 0 & 0 & 0 \end{bmatrix},$$

$$\Phi = \begin{bmatrix} \varphi_{1,n} & 0 & -\varphi_{1,n} & 0 & 0 & 0\\ 0 & \varphi_{2,n} & 0 & -\varphi_{2,n} & 0 & 0\\ -\varphi_{1,n} & 0 & \varphi_{1,n} & 0 & 0 & 0\\ 0 & -\varphi_{2,n} & 0 & \varphi_{2,n} & 0 & 0\\ 0 & 0 & 0 & 0 & 0 & 0\\ 0 & 0 & 0 & 0 & 0 & 0 \end{bmatrix}, \quad X_n = \begin{bmatrix} X_{1,n}\\ Y_{1,n}\\ X_{2,n}\\ Y_{2,n}\\ \phi_{1,n}\\ \phi_{2,n} \end{bmatrix}, \phi(X_n) = \begin{bmatrix} \frac{a}{1+x_{1,n}^2}\\ \eta\sigma\\ \frac{a}{1+x_{2,n}^2}\\ \eta\sigma\\ 0\\ 0 \end{bmatrix}$$

$\Psi(x)$ is continuous and consequently satisfies Lipschitz condition [32], i.e:

$$\forall X, \bar{X} \in S, \ \exists \zeta_1 \geqslant 0 \quad \text{s.t} \ \ \|(\Psi(x) - \Psi(\bar{x})\| \leqslant \zeta_1 \|x - \bar{x}\| \tag{2.7}$$

We now prove that the system (2.5) satisfies the locally Lipschitz condition:

$$\forall X, \bar{X} \in S,\ \exists L \geqslant 0 \quad \text{s.t} \ \ \|\mathbb{F}(X) - \mathbb{F}(\bar{X})\| \leqslant L\|X - \bar{X}\|,$$

where $n_1, n_2 \in N_1, n_1 < n_2$,

$$\begin{aligned} \left\|F(X) - F(\overline{X})\right\| &= \left\|\Psi(X) - \Psi(\overline{X}) + A(X - \overline{X}) + k\Phi(X - \overline{X})\right\| \\ &\leqslant \|\Lambda\| \left\|X - \overline{X}\right\| + \|A\| \left\|X - \overline{X}\right\| + k \|\Phi\| \left\|X - \overline{X}\right\| \leqslant \ L \left\|X - \overline{X}\right\| \end{aligned}$$

and

$$\begin{aligned} L &= (\|A\| + (2k+1)\ \|\Lambda\|), \\ X &= \left(x_{1,n_1}, y_{1,n_1}, x_{2,n_1}, y_{2,n_1}, \phi_{1,n_1}, \phi_{2,n_1}\right), \\ \overline{X} &= \left(\overline{x}_{1,n_2}, \overline{y}_{1,n_2}, \overline{x}_{2,n_2}, \overline{y}_{2,n_2}, \overline{\phi}_{1,n_2}, \overline{\phi}_{2,n_2}\right). \end{aligned}$$

This means that with an initial condition $X_0 = (x_{1,0}, y_{1,0}, x_{2,0}, y_{2,0}, \phi_{1,0}, \phi_{2,0})^T$, the network model (2.5) has a unique solution $X_n \in S$. □

2.2.2. Stability analysis

This section provides a comprehensive theoretical foundation for analyzing stability.

Definition 2.8. [33] The inverse Laplace transform of a function $f : \mathbb{N} \to \mathbb{C}$ is

$$\aleph_a[f(n)] = \sum_{k=1}^{\infty} f(n_k)(1-s)^{k-1} \tag{2.8}$$

where the series converges for all the points $s \in \mathbb{C}$.

Definition 2.9. [34] The Mittag-Leffler function for matrix arguments is

$$F_\alpha(B, (n-a)^{\overline{\alpha}}) = \sum_{k=0}^{\infty} \frac{(n-a)^{\overline{\alpha k}}}{\Gamma(\alpha k + 1)} B^k$$

where the spectral radius of the matrix B is less than 1, $n \in N_a$, $0 < \alpha < 1$, and $B \in R^{k\times k}$.

Definition 2.10. [34] In fractional nabla calculus, the matrix exponential function for a matrix $B \in R^{k\times k}$ is

$$e_{\alpha,\alpha}(B, (n-a)^{\overline{\alpha}}) = \sum_{k=0}^{\infty} (n-a+1)^{\overline{\alpha(k+1)}} B^k (I - B)$$

where the spectral radius of the matrix B is less than 1, $n \in N_a$ and $0 < \alpha < 1$.

Lemma 2.11. *[25] Asymptotic stability of the linear system $\nabla x(n) = Bx(n)$ is guaranteed if and only if every root of the characteristic equation, $p(\lambda) = \lambda^2 - b\lambda + c$ is contained within the unit disk.*

Lemma 2.12. *[36] The linear system* ${}_a^C\nabla^\beta x(n) = Bx(n)$ *exhibits asymptotic stability if and only if the set of eigenvalues of matrix B is confined to*

$$S_\beta = \{w \in \mathbb{C} : |\arg(w)| > \frac{\beta\pi}{2} \text{ or } |w| > (2\cos(\arg(w)/\beta))^\beta\} \tag{2.9}$$

where $x(n) \in \mathbb{R}^k$, $B \in \mathbb{R}^{k\times k}$ *and* $0 < \beta < 1$.

Lemma 2.13. *[35] The following statement is valid*

$$e_{\alpha,\alpha}(n^{\overline{\alpha}}) = (n+1)^{\overline{\alpha-1}} F_{\alpha,\alpha}(\lambda, (n+\alpha)^{\overline{\alpha}}) \tag{2.10}$$

Lemma 2.14. *[33] Let* $0 < \alpha < 1$ *and* $\lambda \in S_\alpha$. *Then, the discrete Mittag-Leffler function exhibits the subsequent property*

$$F_\alpha(\lambda, n) = O(n^{-\alpha}) \quad as \quad n \to \infty. \tag{2.11}$$

Lemma 2.15. *[36] Let* $0 < \alpha < 1$, *if any of the following conditions hold, the roots of* $p(\lambda) = \lambda^2 - b\lambda + c$ *belong to* S_α

i . $c > 4^\alpha$ and $b < 2^{-\alpha}c + 2^\alpha$

ii . $0 < c \leqslant 4^\alpha$ and $c < 2\sqrt{c}\cos\left(\alpha \arccos\left(\frac{1}{2}\sqrt{c}\right)\right)$

iii .$c < 0$ and $b > 2^{-\alpha}c + 2^\alpha$.

2.3. Equilibrium Analysis

To determine the steady-state of the FDMCRN, we set the nabla fractional differences of the state variables to zero, ${}_a^C\nabla^\alpha x_i(n) = 0$, ${}_a^C\nabla^\alpha y_i(n) = 0$, ${}_a^C\nabla^\alpha \varphi_i(n) = 0$ for $i = 1, 2$. By substituting the model equations, the set of equilibrium points E^* is identified as:

$$E^* = \left(\sigma, \sigma - \frac{a}{\sigma^2+1}, \sigma, \sigma - \frac{a}{\sigma^2+1}, \gamma_1, \gamma_2\right) \tag{2.12}$$

where $\gamma_1, \gamma_2 \in \mathbb{R}$ are arbitrary constants representing the magnetic fluxes. The existence of these constants indicates that the system possesses a line of equilibrium. This characteristic implies that the steady-state of the FDMCRN is sensitive to its initial conditions, which is a direct consequence of the memory effect inherent in memristive synapses.

To establish the stability criteria for the FDMCRN model, we adopt the general framework of discrete fractional-order stability for nonlinear systems. Analyzing nonlinear discrete fractional-order systems is inherently challenging; therefore, we focus on local asymptotic stability, which is evaluated by examining the eigenvalues of the Jacobian matrix at the equilibrium points. In this procedure, the nonlinear map is approximated by its linearization around the steady state. By invoking Lemma 2.12, which provides necessary and sufficient conditions for the stability of linear nabla discrete fractional systems, we can define a stability criterion applicable to a broad class of nonlinear fractional-order systems. The following theorem applies to both the two-neuron configuration and its extension to a ring network.

Theorem 2.16. *The fractional order system*

$$ {}_{a}^{C}\nabla^{\alpha} X(n) = BX(n) + \mathbb{H}[X(n)] \tag{2.13} $$

asymptotic stability in the vicinity of its equilibrium point $X^{\star}$*, given the conditions*

$$ \lambda_i \in S_\alpha \quad \text{and} \quad \lim_{X \to X^{\star}} \frac{\| \mathbb{H}[X(n)] \|}{\|X(n) - X^{\star}(n)\|} = 0, $$

where $\mathbb{H}[X(n)]$ *is a nonlinear term,* λ_i *are the eigenvalues of matrix* $B \in R^{k \times k}$ *and* $X(n) \in R^{k \times 1}$.

Proof. According to the method proposed in [34], the unique solution of (2.13) is expressed as

$$ X(n) = F_\alpha(B, n^{\overline{\alpha}})X(n_0) + \sum_{s=1}^{n} e_{\alpha,\alpha}(B, (n-s)^{\overline{\alpha}})(I - B)^{-1} H(X(n)), $$

Suppose $X^{\star}$ is the solution of system (2.13), Hence For every $\varepsilon > 0$, there exists $\delta_0 > 0$ such that if $\|X(n) - X^{\star}\| < \delta_0$ then $\| \mathbb{H}[X(n)] \| < \varepsilon \|X(n) - X^{\star}\|$. Thus,

$$ \|X(n) - X^{\star}\| \leqslant \left\|F_\alpha(B, n^{\overline{\alpha}})\right\| \|X(n_0)\| + \sum_{s=1}^{n} \varepsilon \left\| e_{\alpha,\alpha}(B, (n-s)^{\overline{\alpha}}) \right\| \|I - B\|^{-1} \|X(n) - X^{\star}\|, $$

Given that δ is chosen arbitrarily such that $0 < \delta < \delta_0$, and considering lemma 2.13 we can derive

$$ \|X(n) - X^{\star}\| \leqslant \delta \left\|F_\alpha(B, n^{\overline{\alpha}})\right\| + M \sum_{s=1}^{n} (n+1)^{\overline{\alpha-1}} \left\| F_\alpha(B, (n+\alpha-s)^{\overline{\alpha}}) \right\|, $$

where $M = \varepsilon\delta_0(1 + \|B\|)^{-1}$, regarding $(n+1)^{\overline{\alpha-1}} = \frac{n^{\overline{\alpha}}}{n+1}$ proves that $\frac{n^{\overline{\alpha}}}{n+1} = O(n^{\alpha-1})$, by lemma 2.14 we have

$$ \|X(n) - X^{\star}\| \leqslant \ell_1 n^{-\alpha} + \ell_2 n^{\alpha-1} \sum_{s=1}^{n} (n)^{-1-\alpha}, $$

$$ \|X(n) - X^{\star}\| \leqslant \ell_1 n^{-\alpha} + \ell_2 \ell_3 n^{-1}, $$

$$ \|X(n) - X^{\star}\| \to 0 \quad \text{as} \quad n \to \infty, $$

Asymptotic stability of the solution of system (2.13) is suggested by this result. □

2.3.1. Stability Analysis of the FDMCRN model

In this section, the local stability of the proposed fractional-order discrete memristive coupling Rulkov network is investigated.

Theorem 2.17. *The system* (2.4) *exhibits asymptotic stability at its equilibrium point,* $E^* = (\sigma, \sigma - \frac{a}{\sigma^2+1}, \sigma, \sigma - \frac{a}{\sigma^2+1}, \gamma_1, \gamma_2)$ *where* γ_1, γ_2 *are constants representing specific positions on*

the line of equilibrium points, if and only if, in each case, any of the following conditions holds true

***Case1**:*

i . $c_0 > 4^\alpha,\ \ 2^\alpha - 2^{-\alpha}\eta < \vartheta - k\gamma_1$

ii . $0 < c_0 \leqslant 4^\alpha,\ \ -2\,\eta^{\frac{1}{2}}\cos(\frac{\alpha}{2}\cos^{-1}(\eta^{\frac{1}{2\alpha}})) < \vartheta - k\gamma_1$

iii . $c_0 < 0,\ \ 2^\alpha - 2^{-\alpha}\eta > \vartheta - k\gamma_1$

***Case2**:*

i . $b_0 > 4^\alpha,\ \ \vartheta + k\gamma_1 + 2k\gamma_2 < 2^{1-\alpha}(k\gamma_1{\gamma_2}^2 - \vartheta k\gamma_2) - 2^\alpha$

ii . $0 < b_0 \leqslant 4^\alpha,\ \ \vartheta + k\gamma_1 + 2k\gamma_2 < 2\cos[\frac{\alpha}{2}\cos^{-1}[(2k^2\gamma_1\gamma_2 + 2\vartheta k\gamma_2)^{\frac{1}{2\alpha}})]](2k^2\gamma_1\gamma_2 + 2\vartheta k\gamma_2)^{\frac{1}{2}}$

iii . $b_0 < 0,\ \ \vartheta + k\gamma_1 + 2k\gamma_2 < 2^{1-\alpha}(k\gamma_1{\gamma_2}^2 - \vartheta k\gamma_2) - 2^\alpha$

where $0 < \alpha < 1$, $\vartheta = \frac{k\gamma_1 - 2a\sigma}{(\sigma^2+1)^2} - 1$ *and* $b_i, c_i, (i = 0, 1)$ *are listed in Appendix Appendix A.*

Proof. The system (2.4) has the following Jacobian matrix

$$\begin{bmatrix} \frac{k\varphi_1 - 2ax_1}{({x_1}^2+1)^2} - 1 & 1 & -k\varphi_1 & 0 & k(x_1 - x_2) & 0 \\ -\eta & k\varphi_2 & 0 & -k\varphi_2 & k(y_1 - y_2) & 0 \\ -k\varphi_1 & 1 & \frac{k\varphi_1 - 2ax_1}{({x_1}^2+1)^2} - 1 & 0 & -k(x_1 - x_2) & 0 \\ 0 & -k\varphi_2 & -\eta & k\varphi_2 & -k(y_1 - y_2) & 0 \\ 1 & 0 & -1 & 0 & 0 & 0 \\ 0 & 1 & 0 & -1 & 0 & 0 \end{bmatrix} \tag{2.14}$$

which at its equilibrium, will be

$$J(E^\star) = \begin{bmatrix} \frac{k\gamma_1 - 2a\sigma}{(\sigma^2+1)^2} - 1 & 1 & -k\gamma_1 & 0 & 0 & 0 \\ -\eta & k\gamma_1 & 0 & -k\gamma_1 & 0 & 0 \\ -k\gamma_1 & 1 & \frac{k\gamma_1 - 2a\sigma}{(\sigma^2+1)^2} - 1 & 0 & 0 & 0 \\ 0 & -k\lambda_1 & -\eta & k\gamma_1 & 0 & 0 \\ 1 & 0 & -1 & 0 & 0 & 0 \\ 0 & 1 & 0 & -1 & 0 & 0 \end{bmatrix} \tag{2.15}$$

Assuming a_i (i = 0 to 3) and b_i, c_i (i = 0, 1) presented in Appendix Appendix A, The Jacobian matrix's characteristic equation is represented as $p(\lambda) = \lambda^2 p_1(\lambda)$ where

$$p_1(\lambda) = \lambda^4 + a_3\lambda^3 + a_2\lambda^2 + a_1\lambda + a_0 \tag{2.16}$$

by splitting the quartic polynomial by factoring it into two quadratics we can rewrite $p_1(\lambda)$ in the form of

$$p_1(\lambda) = (\lambda^2 + b_1\lambda + b_0)(\lambda^2 + c_1\lambda + c_0) = p_2(\lambda) \times p_3(\lambda) \tag{2.17}$$

According to lemma (2.15) and Theorem 2.16, the proof follows directly.
The analytical expressions for the coefficients of the characteristic polynomials $p_1(\lambda)$, $p_2(\lambda)$ and $p_3(\lambda)$ are provided in Appendix Appendix A due to their algebraic complexity. These coefficients are used to evaluate the stability criteria at the equilibrium points. □

Remark 2.18. The roots of $p_i(\lambda), (i = 1, 2, 3)$ must be located in the region S_α which is shown in Fig. 3.

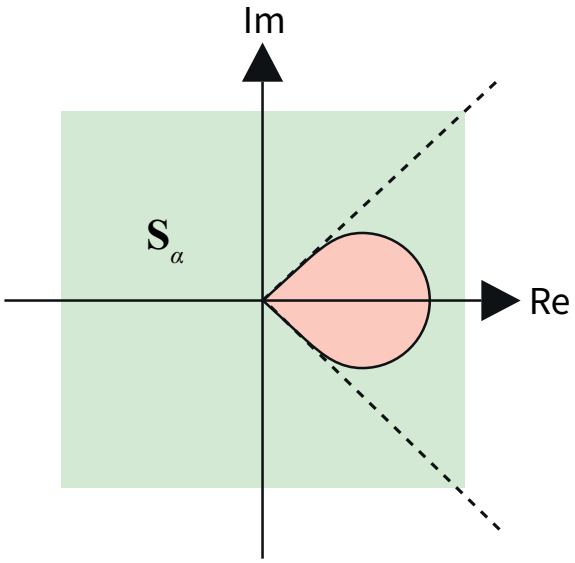

Figure 3: Asymptotic stability region S_α.

2.3.2. Stability Analysis of the FDMCRN Ring Network

Before analyzing the stability of the ring network, it is important to understand that this configuration extends the two-neuron FDMCRN model by interconnecting N units in a symmetric ring. Each unit interacts with its P nearest neighbors through memristive couplings, which introduces additional collective dynamics not present in the isolated two-neuron system. Applying the general stability Theorem 2.20 allows us to investigate how these interactions influence local asymptotic stability across the entire network.

Remark 2.19. Assume $\blacksquare = \mathrm{bcirc}(\mathbf{T}, \tau, ..., \tau) \in \mathbb{C}^{N\times N}$ then [15]

$$\lambda(\blacksquare) = \left\{ \lambda(\mathbf{T} + (N-1)\tau), \underbrace{\lambda(\mathbf{T} - \tau), ..., \lambda(\mathbf{T} - \tau)}_{N-1} \right\}.$$

Theorem 2.20. *The system* (2.5) *exhibits asymptotic stability at its equilibrium point,* $E^* = (\sigma, \sigma^*, \sigma, \sigma^*, \gamma_1, \gamma_2)$*, if and only if, in each case, any of the following conditions holds true*

Case1*:*

i . $N-1 > 4^{\alpha}, -(3D+2P-DN)/(2P) < 2^{-\alpha}(N-1)+2^{\alpha}$

ii . $0 < N-1 < 4^{\alpha}, -(3D+2P-DN)/(2P) < \cos(\alpha\cos^{-1}\frac{(N-1)^{\frac{1}{2\alpha}}}{2})$

Case2*:*

i . $\eta(N-1)^2 > 4^{\alpha}, -(\eta(N-1)^2) < 2^{-\alpha}(\eta(N-1)^2)+2^{\alpha}$

ii . $0 < \eta(N-1)^2 < 4^{\alpha}, -(\eta(N-1)^2)/(2P) < \cos(\alpha\cos^{-1}\frac{(N-1)^{\frac{1}{2\alpha}}}{2})$

Case3*:*

i . $N-1 > 4^{\alpha}, (3D+2P-3DN-2NP)/(2P) < 2^{-\alpha}(N-1)+2^{\alpha}$

ii . $0 < N-1 < 4^{\alpha}, (3D+2P-3DN-2NP)/(2P) < \cos(\alpha\cos^{-1}\frac{(N-1)^{\frac{1}{2\alpha}}}{2})$

where $\alpha \in (0,1)$.

Proof. Compact form of the network (2.5) is presented as $\mathbb{F}(X) = \mathbb{A}X + \mathbb{H}(X)$, matrix $A \in \mathbb{R}^{N\times N}$ is a block circulant matrix constructed from the blocks $A_0, A_1, ..., A_1$, such that $A_0, A_1 \in \mathbb{R}^{6\times 6}$, $\mathbb{H}(X) = \Psi(X) + k\widetilde{\Phi}X$ and $\widetilde{\Phi} = \text{bcirc}(\Phi, 0, .., 0)_{1\times N}$ as

$$\mathbb{A}_0 = \begin{bmatrix} -1-D/P & 1 & 0 & 0 & 0 & 0 \\ -\eta & 0 & 0 & 0 & 0 & 0 \\ 0 & 0 & -1 & 1 & 0 & 0 \\ 0 & 0 & -\eta & 0 & 0 & 0 \\ 1 & 0 & -1 & 0 & 0 & 0 \\ 0 & 1 & 0 & -1 & 0 & 0 \end{bmatrix},$$

$$\mathbb{A}_1 = \begin{bmatrix} D/2P & 0 & 0 & 0 & 0 & 0 \\ 0 & 0 & 0 & 0 & 0 & 0 \\ 0 & 0 & 0 & 0 & 0 & 0 \\ 0 & 0 & 0 & 0 & 0 & 0 \\ 0 & 0 & 0 & 0 & 0 & 0 \\ 0 & 0 & 0 & 0 & 0 & 0 \end{bmatrix},$$

$$\Psi(X_n) = \begin{bmatrix} \frac{a}{1+x_{1,n}^2} \\ \eta\sigma \\ \frac{a}{1+x_{2,n}^2} \\ \eta\sigma \\ 0 \\ 0 \end{bmatrix}, \quad \Phi = \begin{bmatrix} \varphi_1 & 0 & -\varphi_1 & 0 & 0 & 0 \\ 0 & \varphi_2 & 0 & -\varphi_2 & 0 & 0 \\ -\varphi_1 & 0 & \varphi_1 & 0 & 0 & 0 \\ 0 & -\varphi_2 & 0 & \varphi_2 & 0 & 0 \\ 0 & 0 & 0 & 0 & 0 & 0 \\ 0 & 0 & 0 & 0 & 0 & 0 \end{bmatrix},$$

Next, we prove that equation (2.5) meets the stability condition at its equilibrium point, because

$$\lim_{X\to X^*}\frac{\|\mathbb{H}(X)\|}{\|X-X^\star\|}=\lim_{X\to X^*}\frac{k\left\|\widetilde{\Phi}\right\|\|X\|}{\|X-X^\star\|}=0,$$

and using Remark 2.19, we have

$$p(\lambda)=\det(\mathbb{A}-\lambda I)=\{p_1(\lambda)\times p_2(\lambda)\},$$

$$p_1(\lambda)=\lambda^2(\lambda^4+a_3\lambda^3+a_2\lambda^2+a_1\lambda+a_0), \tag{2.18}$$

$$p_2(\lambda)=\lambda^2(\lambda^4+b_3\lambda^3+b_2\lambda^2+b_1\lambda+b_0), \tag{2.19}$$

By factoring each of the quartic polynomials into two quadratic factors, we can rewrite

$$\begin{aligned}p_1(\lambda)&=\lambda^2(\lambda^2+s_1\lambda+s_0)(\lambda^2+u_1\lambda+u_0),\\ p_2(\lambda)&=\lambda^2(\lambda^2+q_1\lambda+q_0)(\lambda^2+v_1\lambda+v_0),\end{aligned}$$

where

$$\begin{cases}s_1=(-3D-2P+3DN+2NP)/(2P)\\ s_0=N-1\\ u_1=\eta N^2-2N\eta+\eta\\ u_0=\eta N^2-2N\eta+\eta\end{cases}\qquad\begin{cases}q_1=(3D+2P-DN)/(2P)\\ q_0=N-1\\ v_1=\eta N^2-2N\eta+\eta\\ v_0=\eta N^2-2N\eta+\eta\end{cases}$$

The full analytical expressions for the coefficients of the characteristic polynomials $p_1(\lambda)$ and $p_2(\lambda)$ are provided in Appendix Appendix B and by applying Lemma (2.15) and Theorem 2.16, the proof becomes straightforward. □

3. Numerical Simulation

In this section, we conduct comprehensive numerical simulations to validate the theoretical stability criteria established in the previous sections. To this end, two distinct examples are presented: the first focuses on a two-neuron model while the second investigates the dynamics of a structured ring network.

3.1. Computational Implementation via Nabla Fractional Differences

To investigate the dynamical characteristics of the proposed systems, we transform the nabla fractional difference equations into a computationally traceable form. The numerical solution for a Nabla system ${}_0^C\nabla^\alpha X(n)=f(X(n))$ is given by the following fractional

sum [23]:

$$X(n) = X(0) + \frac{1}{\Gamma(\alpha)} \sum_{j=1}^{n} \frac{\Gamma(n-j+\alpha)}{\Gamma(n-j+1)} f(X(j)). \tag{3.1}$$

By applying the aforementioned numerical scheme, the fractional-order Rulkov network described in model (2.4) is discretized as follows:

$$\begin{cases} x_1(n) = x_1(0) + \frac{1}{\Gamma(\alpha)} \sum_{j=1}^{n} \mathcal{G}(n,j) \left[\frac{a}{1+x_1^2(j)} + y_1(j) + k\varphi_1(j)(x_1(j) - x_2(j)) - x_1(j) \right], \\ y_1(n) = y_1(0) + \frac{1}{\Gamma(\alpha)} \sum_{j=1}^{n} \mathcal{G}(n,j) \left[-\eta(x_1(j) - \sigma) + k\varphi_2(j)(y_1(j) - y_2(j)) \right], \\ x_2(n) = x_2(0) + \frac{1}{\Gamma(\alpha)} \sum_{j=1}^{n} \mathcal{G}(n,j) \left[\frac{a}{1+x_2^2(j)} + y_2(j) - k\varphi_1(j)(x_1(j) - x_2(j)) - x_2(j) \right], \\ y_2(n) = y_2(0) + \frac{1}{\Gamma(\alpha)} \sum_{j=1}^{n} \mathcal{G}(n,j) \left[-\eta(x_2(j) - \sigma) - k\varphi_2(j)(y_1(j) - y_2(j)) \right], \\ \varphi_1(n) = \varphi_1(0) + \frac{1}{\Gamma(\alpha)} \sum_{j=1}^{n} \mathcal{G}(n,j) \left[x_1(j) - x_2(j) \right], \\ \varphi_2(n) = \varphi_2(0) + \frac{1}{\Gamma(\alpha)} \sum_{j=1}^{n} \mathcal{G}(n,j) \left[y_1(j) - y_2(j) \right], \end{cases} \tag{3.2}$$

where $\mathcal{G}(n,j)$ accounts for the power-law fading memory and is defined using the Gamma function:

$$\mathcal{G}(n,j) = \frac{\Gamma(n-j+\alpha)}{\Gamma(n-j+1)}. \tag{3.3}$$

This numerical approach is systematically extended to analyze the dynamics of the ring network configuration model (2.5).

Particular Scenario: Example I

This example is provided to illustrate the practical application of the stability conditions derived in this study. Specifically, we consider model (2.4) under the parameter configuration $a = 3$, $k = 0.05$, $\mu = 0.001$, and $\sigma = -1.5$. Consequently, the equation (2.16) simplifies to

$$p_1(\lambda) = (\lambda^2 + b_1\lambda + b_0)(\lambda^2 + c_1\lambda + c_0) \tag{3.4}$$

Under the assumptions

$$b_1 = \frac{25 - 185\gamma_1 k}{169} - 2\gamma_2 k, \; b_0 = 2\gamma_2 \left(\frac{k}{169}(16\gamma_1 k - 25) + \gamma_1 k^2 \right),$$

$$c_1 = \frac{153\gamma_1 k + 25}{169}, \; c_0 = 0.001,$$

the stability criteria stated in Theorem 2.17 are satisfied if and only if

$$0 < c_0 \leqslant 4^{\alpha}, \;\; -c_1 < 2\sqrt{c_0}\cos(\alpha \cos^{-1}\frac{(c_0)^{\frac{1}{2\alpha}}}{2})$$

and provided that any of these qualifications is met

i . $b_0 > 4^{\alpha}, \;\; b_1 > -2^{-\alpha} b_0 - 2^{\alpha}$

Stability conditions based on upper and lower boundary of γ_2			
Fractional order	Condition (1)	Condition (2)	Condition (3)
$\alpha = 0.99$	γ_2 < -119.9058	-4106.6 < γ_2 < -4.8162	γ_2 >0

Table 2: Stability region of two neuron model 2.4 of Example I .

ii . $0 < b_0 \leqslant 4^\alpha$, $-b_1 < 2\sqrt{b_0}\cos(\alpha \cos^{-1}(\frac{(b_0)^{\frac{1}{2\alpha}}}{2}))$

iii . $b_0 < 0$, $b_1 \prec -2^{-\alpha}b_0 - 2^\alpha$.

The above said stability conditions can be expressed in terms of upper and lower bounds of γ_1 and γ_2 values. Then, the stability criteria of model (2.4) is met if and only if

$$\gamma_1 > \frac{169}{153k}(-\frac{25}{169} - 2\sqrt{0.001}\cos(\alpha\cos^{-1}\frac{(0.001)^{\frac{1}{2\alpha}}}{2})) \tag{3.5}$$

and provided that any of these qualifications is met

1 . $2k\gamma_2 R_1 > 4^\alpha$, $k\gamma_2[2 - R_1 2^{-\alpha+1}] < 2^\alpha - R_1$

2 . $0 < 2k\gamma_2 R_1 < 4^\alpha$, $2^{-\alpha}k\gamma_2 + \alpha^2(\frac{\pi}{2} - \frac{(2k\gamma_2 R_1)^{\frac{1}{2\alpha}}}{2})^2 < 1 - R_1 2^{-\alpha-1}$

3 . $2k\gamma_2 R_1 < 0$, $2^\alpha - R_1 < k\gamma_2[2 - R_1 2^{-\alpha+1}]$

where $R_0 = -\frac{25}{169} - 2\sqrt{0.001}\cos(\alpha\cos^{-1}\frac{(0.001)^{\frac{1}{2\alpha}}}{2})$ and $R_1 = \frac{185}{153}R_0 - \frac{25}{169}$.
The model clearly exhibits a line equilibrium point, which is represented as

$$E = (\sigma, \sigma - \frac{a}{\sigma^2+1}, \sigma, \sigma - \frac{a}{\sigma^2+1}, \gamma_1, \gamma_2)$$

where γ_1 and γ_2 are constants that indicate specific positions along the line of equilibrium points. Using the prescribed bounds for γ_1 and γ_2 given in Eq. (3.5) and Table 2, the stability region is mapped and illustrated in Fig. 4. Within this framework, the stability properties of the model are systematically analyzed and discussed under four distinct scenarios.

Scenarios 1: for $\alpha = 0.99$, $\gamma_1 = -1$ and $\gamma_2 = -130$, condition (1) in Table 2 is satisfied. The eigenvalues of the Jacobian matrix can then be determined in the set, Λ= $\{-13, -0.2027, 0, 0, -0.0109, -0.0918\}$. Due to Theorem 2.17, all the eigenvalues are located in S_α, and the system is stable, Fig. 5.

Scenarios 2: for $\alpha = 0.99$, $\gamma_1 = -2$ and $\gamma_2 = -45$, condition (2) in Table 2 is satisfied. The eigenvalues of the Jacobian matrix can subsequently be calculated in the set Λ=$\{-4.5, -0.2574, 0, 0, -0.0287 - 0.0133i, -0.0287 + 0.0133i\}$. According to Theorem. 2.17, for a discrete fractional nabla system to be asymptotically stable, the eigenvalues must lie within the region S_α, Fig. 6.

Scenarios 3: for $\alpha = 0.99$, $\gamma_1 = -3$ and $\gamma_2 = 50$, condition (3) in Table 2 is satisfied. The spectrum of the Jacobian matrix consists of the following eigenvalues

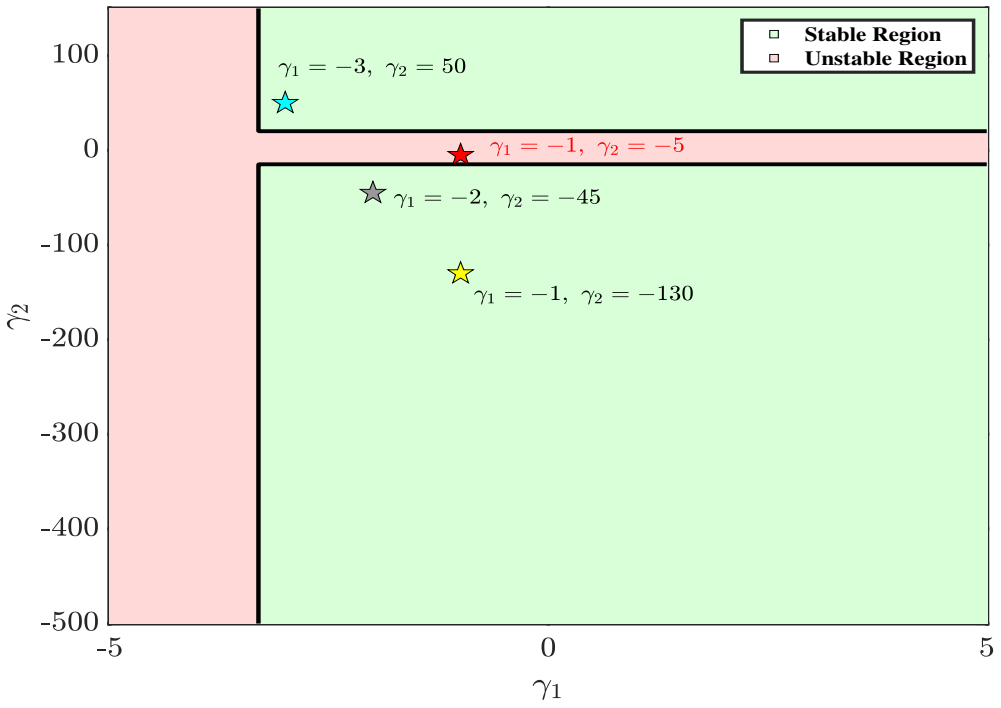

Figure 4: Stability region in the (γ_1, γ_2) plane.

Λ=$\{-0.3121, -0.2574, 0, 0, -0.0061 - 0.0310\mathrm{i}, -0.0061 + 0.0310\mathrm{i}\}$. All the eigenvalues are in S_α and stability is approved, Fig. 7.

Scenarios 4: for $\alpha = 0.99$, $\gamma_1 = -1, \gamma_2 = -5$, the stability criteria are violated. The eigenvalues are $\Lambda = \{-0.5000, -0.2026, 0, 0, -0.0917, -0.0109\}$ and the proximity to the stability boundary suggests a loss of asymptotic stability, leading to the complex oscillations observed in Fig. 8.

Considering different values of α, including $\alpha = 0.79$, $\alpha = 0.89$, $\alpha = 0.99$, from the time series simulation reveals that the time required for the system to stabilize is influenced by the order of the derivative. The closer the order of derivation is to one, the system will reach stability in a shorter time, Fig. 9.

Example II: Ring-Structured Network Analysis

In this subsection, we investigate the collective dynamics of the ring-structured model (2.5) by specifying the network parameters N, P, D, and the fractional order α. For instance, for the parameter set $(\mathrm{P}, \mathrm{D}, \mathrm{N}, \alpha) = (0.1, 0.1, 3, 0.84)$, the system exhibits asymptotic stability. These parameters are chosen in accordance with the stability criteria established in Theorem 2.20, with the corresponding numerical results summarized in Table 3. This asymptotic stability is further confirmed through numerical simulations shown in Fig. 10, where the state trajectories converge to the equilibrium point, in agreement with the analytical predictions of Theorem 2.20.

Building upon these findings, it is essential to examine the underlying mechanisms that

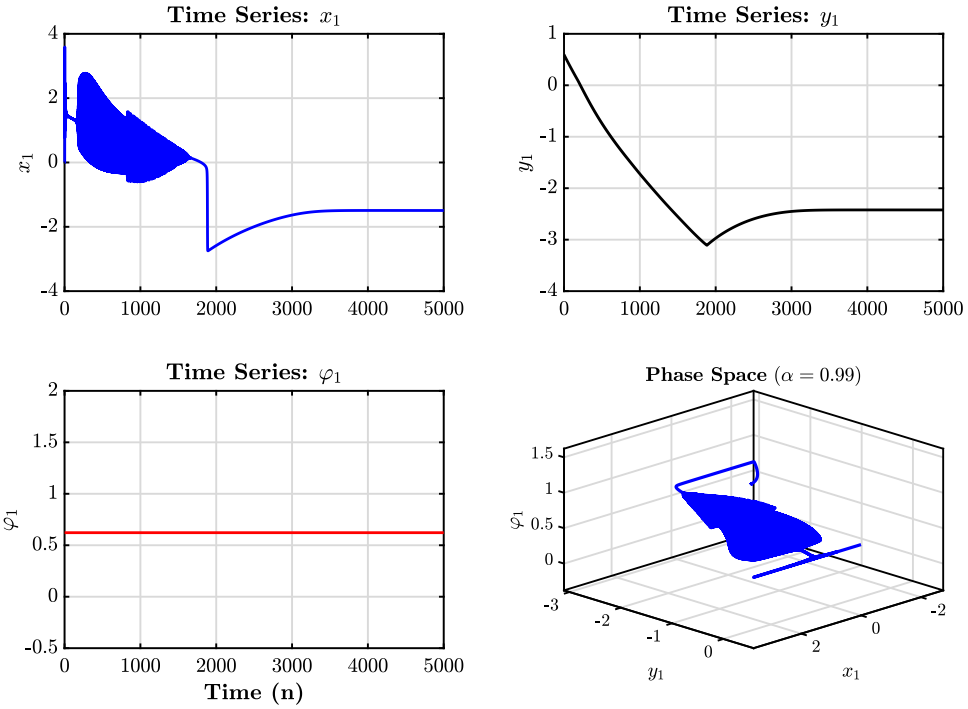

Figure 5: The behavior over time of FDMCRN model (2.4) in Scenario 1, $\alpha = 0.99$.

drive the network's stability. To this end, the following discussion details how these parameters influence the eigenvalues of the Jacobian matrix and, consequently, the stability region defined by Theorem 2.20:

1. **Spectral Properties (**$\mathsf{N}, \mathsf{P}, \mathsf{D}$**):** These parameters collectively define the Jacobian spectrum of the network. We predict that variations in N, P, or D significantly shift the eigenvalue distribution relative to the boundary of S_α. This suggests that network topology and coupling strength are the primary determinants of the system's proximity to the "edge of stability."
2. **Fractional Domain Reconfiguration:** Theorem 2.20 indicates that α acts as a structural modulator for the stability geometry. Changing the fractional order α reconfigures the region S_α, potentially capturing or excluding eigenvalues and thus altering the system's global stability state.

In accordance with the spectral properties derived in Theorem 2.20, the stability of the proposed network (2.5) is governed by the intricate interplay between the network size N, topology parameter P, and coupling strength D. These parameters collectively dictate the position of the Jacobian spectrum relative to the fractional stability boundary $\partial\mathsf{S}_\alpha$.

Impact of Network size N **on Stability Dynamics:** To demonstrate this, we investigate the system's proximity to the "edge of stability" by varying N while fixing $\alpha = 0.84$, $\mathsf{D} = 0.1$, and $\mathsf{P} = 0.1$. In light of the obtained results, it is essential to examine the un-

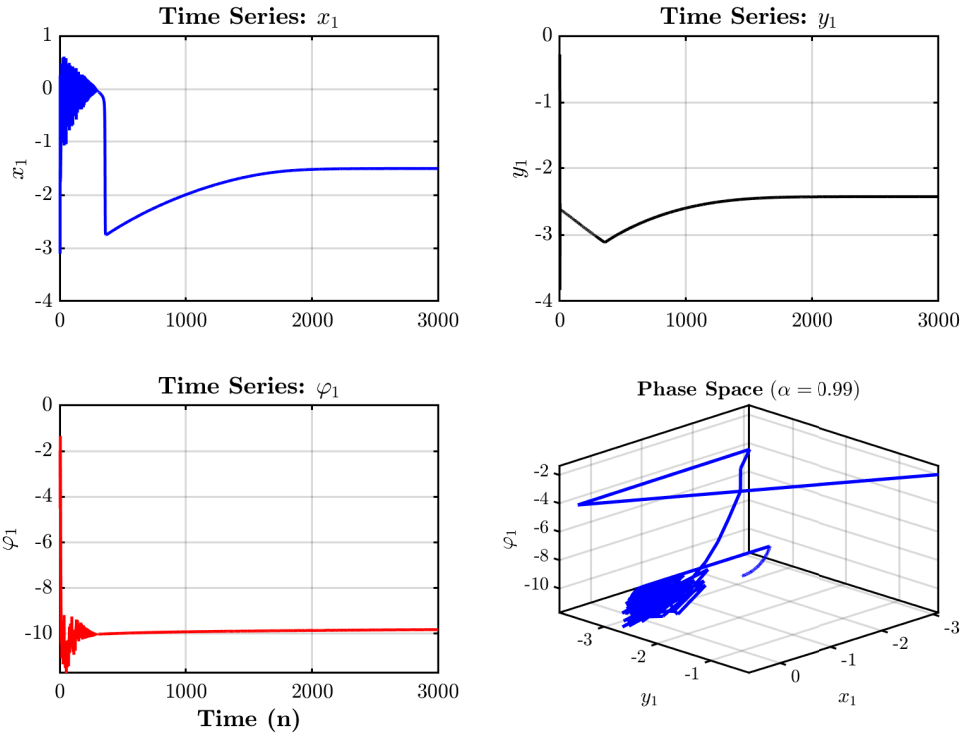

Figure 6: The behavior over time of FDMCRN model (2.4) in Scenario 2, $\alpha = 0.99$.

derlying mechanisms that drive the network's stability. Specifically, we analyze how the variation of the network size N shifts the eigenvalue distribution relative to the fractional stability domain S_α. The following cases summarize the observed transitions:

- **Scenario1 (N = 3):** For a small number of nodes, the eigenvalue spectrum is clustered safely within the interior of the stability region S_α. As illustrated in Fig. 11, all eigenvalues satisfy the stability condition, confirming that the system converges to a Steady-state solution.
- **Scenario2 (N = 7):** As predicted, a variation in N significantly shifts the eigenvalue spectrum toward the periphery. At N = 7, the eigenvalues migrate across the boundary and move into the exterior of the S_α region, Fig. 11. This critical transition represents a topology-induced loss of stability, where the solution becomes unstable.
- **Scenario3 (N = 10):** Further increasing the network size illustrates the re-entrant stability phenomenon. The spectrum shifts again, moving back into the interior of the S_α stability region, Fig. 11. This confirms that the network topology acts as a primary determinant of the asymptotic stability, where a larger N can effectively restore the system to its stable steady-state.

Impact of Network coupling strength D on Stability Dynamics: In this part, we

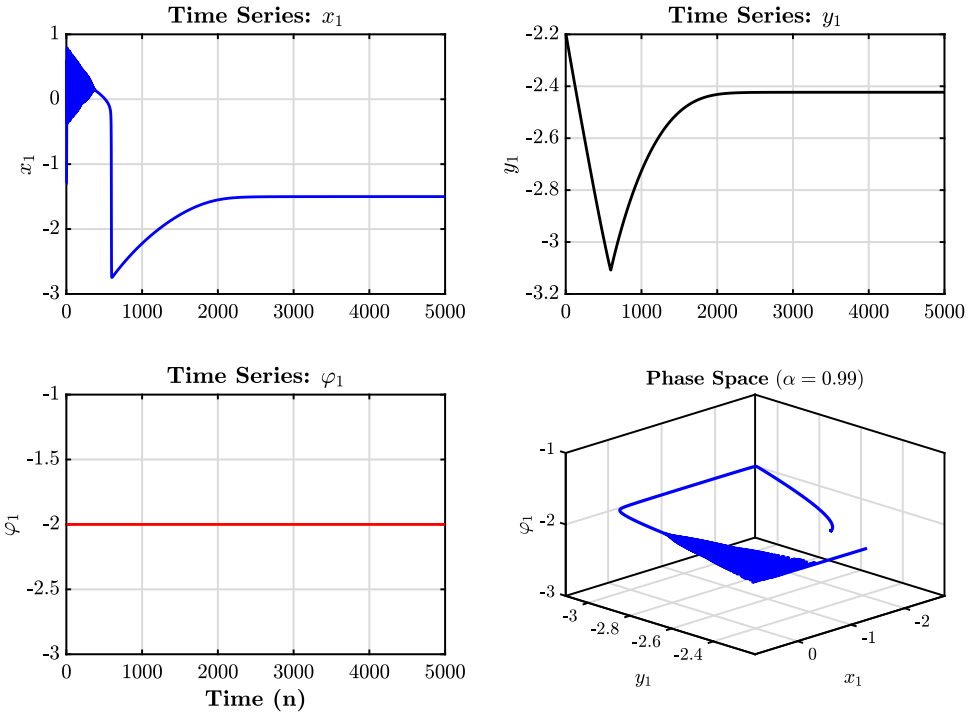

Figure 7: The behavior over time of FDMCRN model (2.4) in Scenario 3 $\alpha = 0.99$.

analyze the migration of the Jacobian spectrum as a function of the coupling strength $D \in [0, 1]$. As depicted in Fig. 12, the network's stability exhibits invariance with respect to the coupling strength D. Despite its role in shifting the eigenvalue distribution, all spectral components remain strictly within the region S_α.

Impact of Network topology parameter P on Stability Dynamics: The network parameter P serves as a topological modulator that scales the influence of synaptic coupling within the Jacobian matrices. To evaluate its effect, we fixed $N = 3$ and $D = 0.1$ while varying $P \in [0, 1]$ across three distinct values, as illustrated in Fig. 13. As P increases within the interval $[0, 1]$, the peripheral eigenvalues shift significantly; however, this spectral movement does not result in a crossing of the fractional stability boundary ∂S_α.

Impact of fractional order α on Stability Dynamics: Unlike the structural parameters D, P, and N, the fractional order α influences the system's stability by reshaping the stability region rather than modifying the eigenvalue locations. As indicated by Theorem 2.20, the Jacobian matrix is independent of α, and therefore the eigenvalues remain fixed in the complex plane, while the stability boundary ∂S_α varies with α. The system remains stable as long as all eigenvalues lie within S_α (see Fig.14). Moreover, α significantly affects the settling time; decreasing α increases the convergence time due to enhanced memory effects. Hence, α acts as a key parameter governing both the geometric stability region and the transient dynamics of the network (Fig. 15).

We now provide a numerical case study to demonstrate the system's behavior when the parameters N, P, and D violate the stability conditions stipulated in Theorem 2.20.

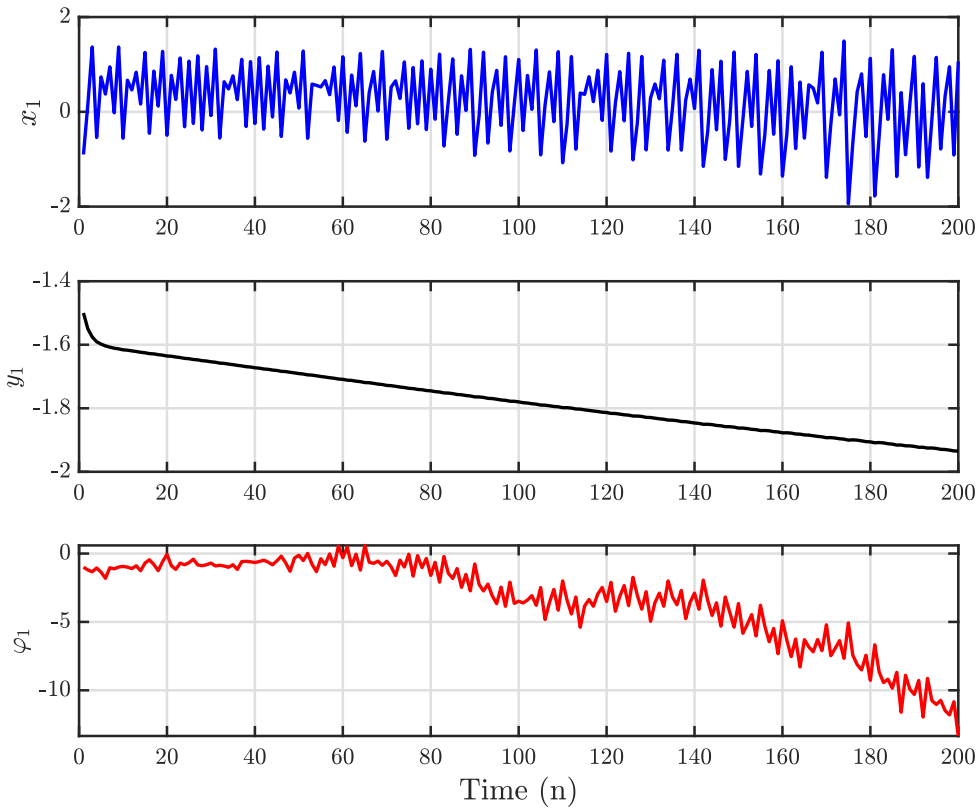

Figure 8: The behavior over time of FDMCRN model (2.4) in Scenario 4, $\alpha = 0.99$.

As illustrated in the following numerical example, once these conditions are breached, the system fails to maintain its asymptotical stability Fig. 16. This case study serves as a practical validation, confirming that the network's stability is not solely dictated by the fractional order α, but emerges from the collective interplay between the underlying topology and the coupling parameters.

4. Discussion and Conclusion

The analytical and numerical results presented in this study provide a robust validation of the proposed discrete fractional-order Rulkov neuron map, integrated with asymmetric memristive synapses and formulated under Caputo's nabla concept. A primary contribution of this work is the theoretical proof of a new stability theorem tailored for nonlinear discrete fractional-order difference equations. By utilizing this theorem, we systematically identified the equilibrium points of the Rulkov model coupled via asymmetric memristors and rigorously determined its stability regions. Unlike conventional symmetric models, the inclusion of asymmetric memristive coupling allows for a more realistic representation of directional synaptic plasticity and electromagnetically induced currents, providing a high-fidelity framework for neural coupling dynamics.

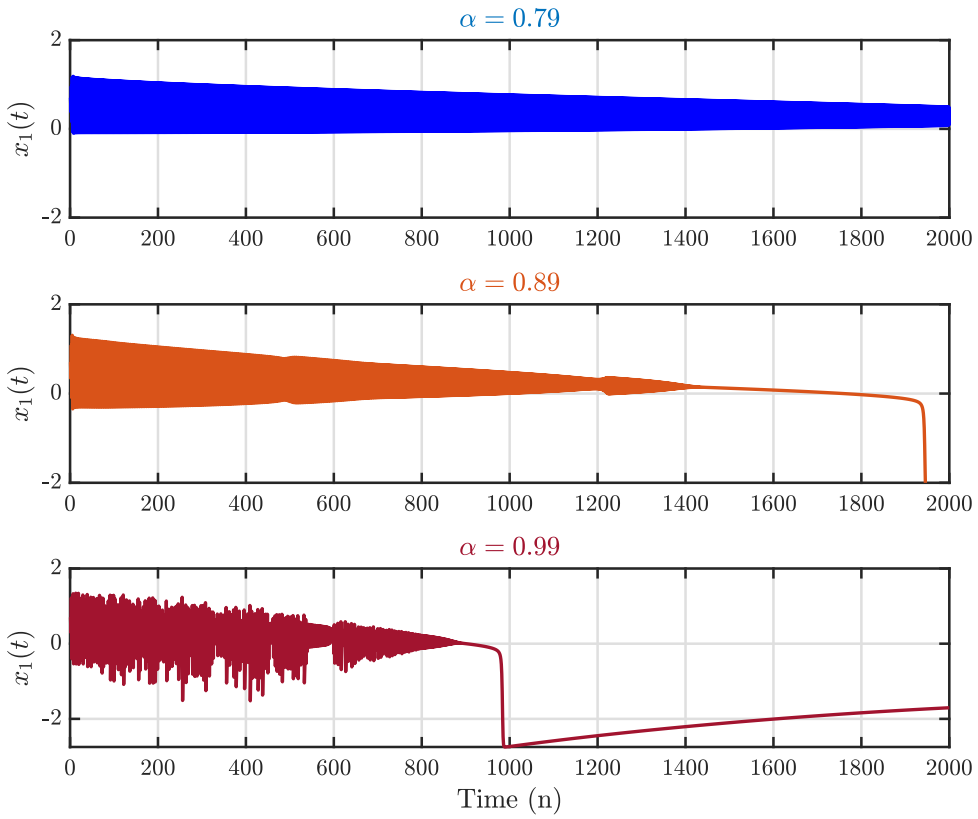

Figure 9: The behavior over time of FDMCRN model 2.4) by three different fractional orders $\alpha = 0.79$, $\alpha = 0.89$, $\alpha = 0.99$.

Furthermore, this study introduced and analyzed a ring-structured network configuration to examine the collective dynamics of neurons under periodic boundary conditions. The stability conditions for this ring-coupled system were investigated, revealing how the network's ring architecture interacts with the asymmetric nature of the synapses to influence the overall spectral distribution. The fractional-order derivatives effectively capture the complex memory effects associated with ion pumping processes, serving as an essential tool to describe the impact of historical states on current neural processing. The numerical investigation of the network with varying parameters, including the number of subnetworks N, the coupling strengths P and D, and the fractional order α, serves as a direct empirical verification of the proven theorem. The boundaries of the stability region are defined by the intricate interplay of these parameters and the asymmetry in the coupling. As demonstrated, the system maintains asymptotic stability as long as these parameters reside within the limits established by the theorem. A significant observation is that the settling time of the system increases as the fractional order α decreases. This is because smaller values of α enhance the memory depth of the system, causing long-range dependence on past states and thereby slowing down the convergence to equilibrium.

Stability region for ring network (2.5)			
Features	Case 1	Case 2	Case 3
$\alpha = 0.84, D = 0.1, P = 0.1, N = 3$	(i) ✗ (ii) ✓	(i) ✗ (ii) ✓	(i) ✗ (ii) ✓

Table 3: Numerical verification of Theorem 2.20 for Cases 1–3. Here, (i) and (ii) represent the first and second stability criteria of the theorem, respectively. The marks ✓ and ✗ indicate whether these criteria are satisfied or violated under the specified parameters N, P, D, and α.

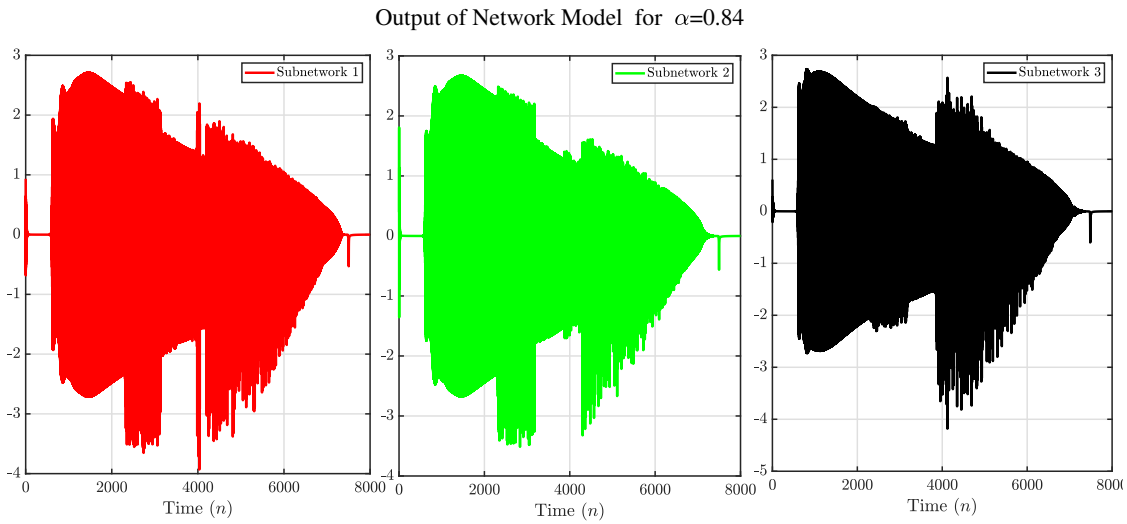

Figure 10: The behavior over time of the model (2.5) based on Table 3 where $\alpha = 0.84, D = 0.1, P = 0.1, N = 3$

In conclusion, this paper has introduced a novel stability framework for discrete fractional-order neural networks and presented a comprehensive stability analysis of the ring-structured model with asymmetric memristors. The results underscore that while asymmetry and topological factors significantly shift the eigenvalue spectrum, the fractional-order damping mechanism enhances the system's robustness against coupling-induced instabilities and influences the convergence time depending on the fractional order. Building on the present findings, investigating alternative fractional-order definitions and synchronization patterns, as well as developing control strategies to optimize convergence and robustness, are promising directions.

Appendix A. The Characteristic Polynomials for Two-Neuron FDMCRN

The full analytical expressions for the coefficients of the characteristic polynomials $p_1(\lambda)$, $p_2(\lambda)$, and $p_3(\lambda)$ for the two-neuron FDMCRN are:

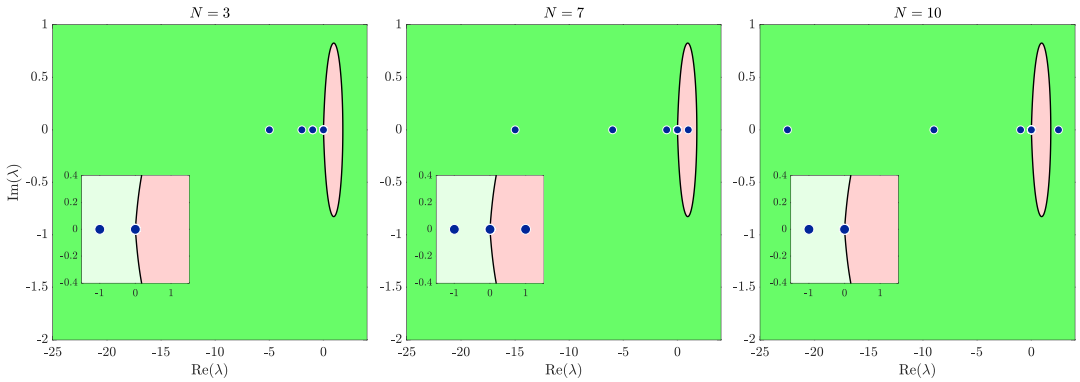

Figure 11: Spectral analysis of the network for $\alpha = 0.84$. The green region represents the stability domain S_α according to Theorem 2.20 red interior corresponds to the instability region. N = 3: Eigenvalues are contained within S_α (Stable). N = 7: Eigenvalues escape the stability boundary due to topological shifts (Unstable). N = 10: The spectrum returns to the interior of S_α (Re-entrant stability).

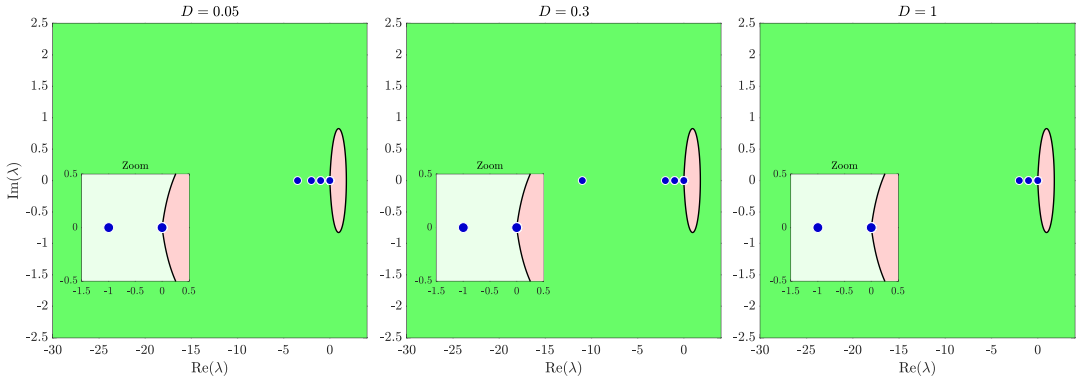

Figure 12: Spectral migration of the Jacobian eigenvalues for N = 3 and $\alpha = 0.84$ as a function of the coupling strength D. The green exterior represents the stable zone S_α, while the red interior corresponds to the instability region. D increases from 0.05 to 1.

Coefficients of $p_1(\lambda)$:

$$a_0 = 2(\gamma_1\gamma_2\eta k^2 + \gamma_2\eta\nu k), \tag{A.1}$$

$$a_1 = -(-2\gamma_2\gamma_1^2 k^3 + \eta\gamma_1 k + 2\gamma_2 k\nu^2 + 2\gamma_2\eta k + \eta\nu), \tag{A.2}$$

$$a_2 = -\gamma_1^2 k^2 + 4\gamma_2 k\nu + \nu^2 + \eta, \tag{A.3}$$

$$a_3 = -(2\nu + 2\gamma_2 k). \tag{A.4}$$

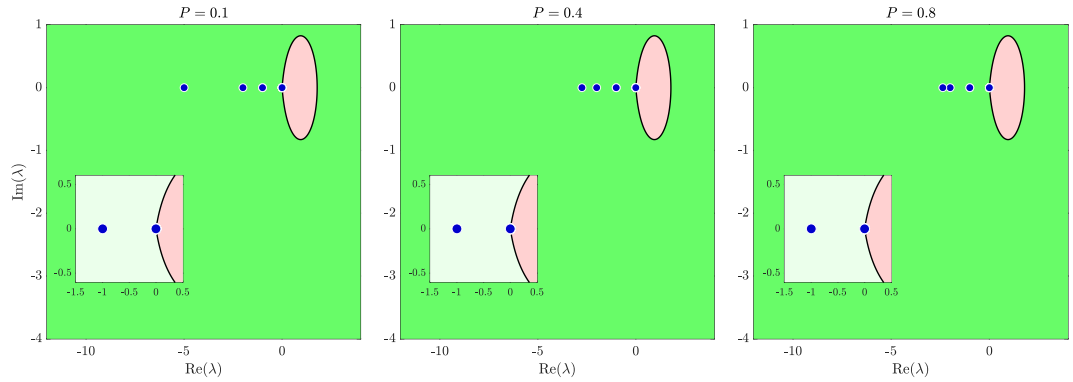

Figure 13: Jacobian eigenvalue distribution as a function of the topology parameter P for $N = 3$, $D = 0.1$, and $\alpha = 0.84$. The green exterior represents the asymptotic stability region, while the red interior signifies the instability domain S_α.

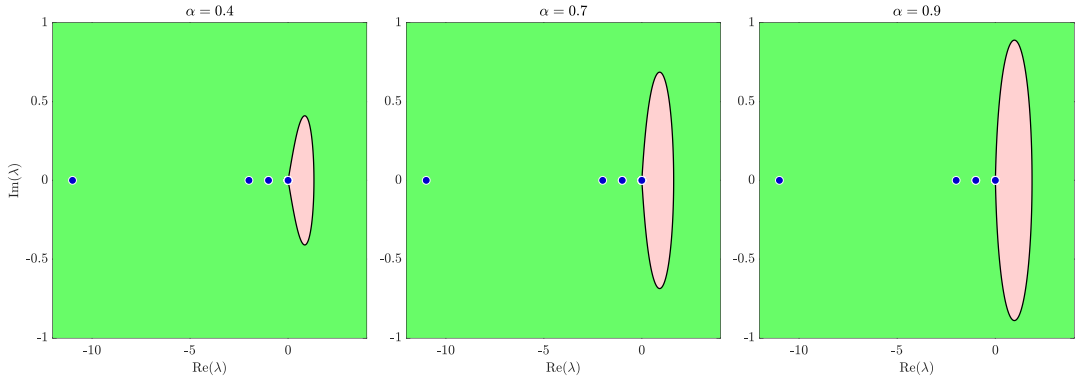

Figure 14: Jacobian eigenvalue distribution in S_α where $\alpha = 0.4$, $\alpha = 0.7$, $\alpha = 0.9$

Coefficients of $p_2(\lambda)$:

$$b_0 = 2\gamma_1\gamma_2 k^2 + 2\gamma_2\vartheta k, \tag{A.5}$$

$$b_1 = -\vartheta - \gamma_1 k - 2\gamma_2 k. \tag{A.6}$$

Coefficients of $p_3(\lambda)$

$$c_0 = \eta, \tag{A.7}$$

$$c_1 = \gamma_1 k - \vartheta. \tag{A.8}$$

Appendix B. The Characteristic Polynomials for Ring-Structured FDMCRN

The full analytical expressions for the coefficients of the characteristic polynomials $p_1(\lambda)$ and $p_2(\lambda)$ for the ring-structured FDMCRN with N neurons are:

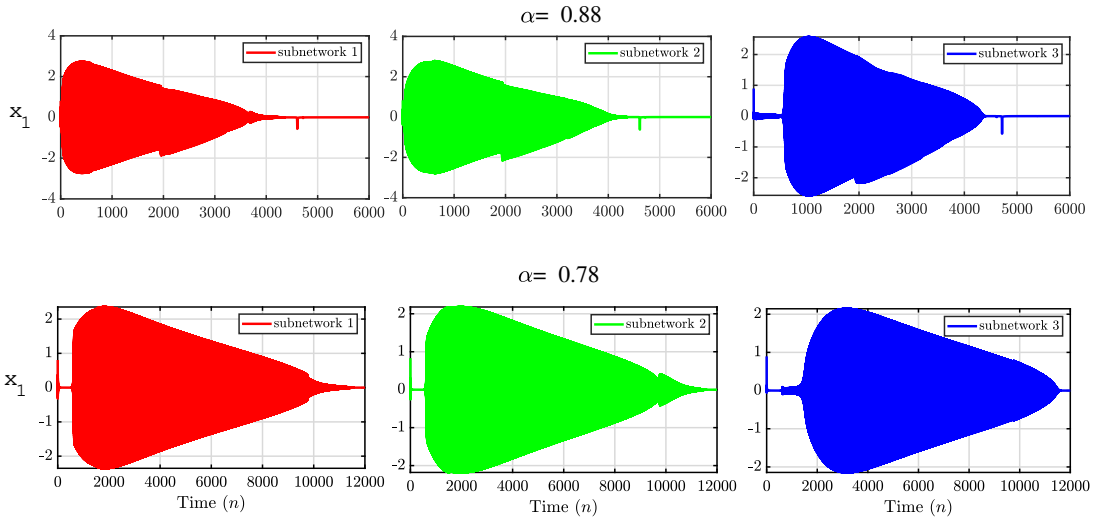

Figure 15: The behavior over time of the model (2.5) in Table 3 where $\alpha = 0.88$, $\alpha = 0.78$

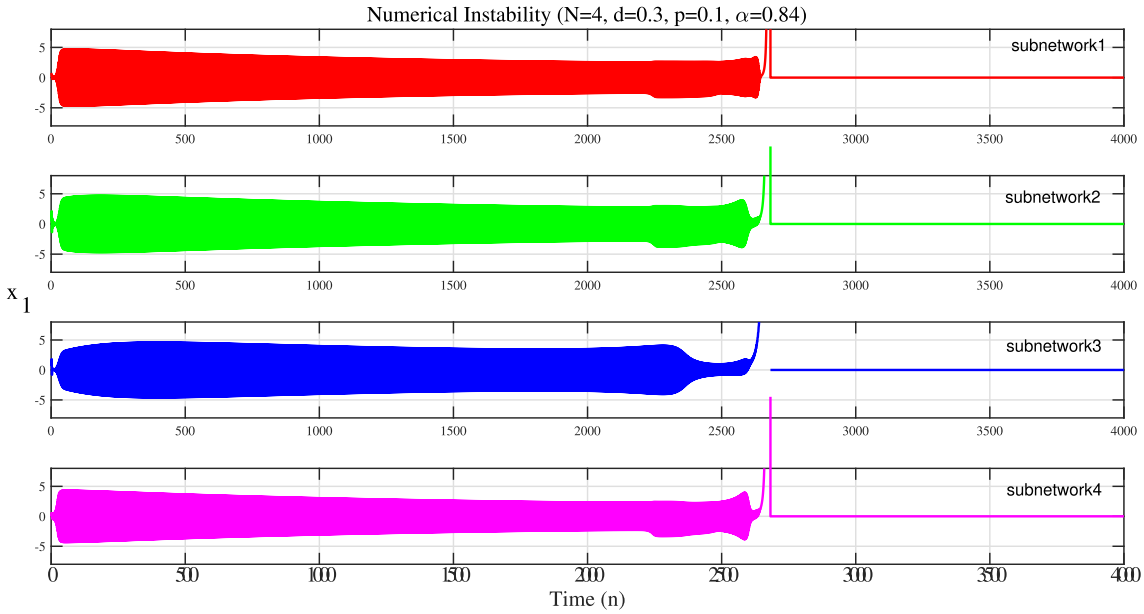

Figure 16: Instability of subnetworks in a ring topology with parameters D = 0.12, N = 4, p = 0.1, $\alpha = 0.84$.

Coefficients of $p_1(\lambda)$:

$$a_0 = \frac{2p\eta^2N^4 - 8p\eta^2N^3 + 12p\eta^2N^2 - 8p\eta^2N + 2p\eta^2}{2p}, \tag{B.1}$$

$$a_1 = -\frac{3d\eta + 4\eta p + 12\eta N^2 p - 4\eta N^3 p - 9d\eta N - 12\eta Np + 9d\eta N^2 - 3d\eta N^3}{2p}, \tag{B.2}$$

$$a_2 = \frac{3d + 2p - 6dN + 4\eta p - 4Np + 3dN^2 + 2N^2 p + 4\eta N^2 p - 8\eta Np}{2p}, \tag{B.3}$$

$$a_3 = -\frac{3d + 4p - 3dN - 4Np}{2p}. \tag{B.4}$$

Coefficients of $p_2(\lambda)$:

$$b_0 = \frac{2p\eta^2N^4 - 8p\eta^2N^3 + 12p\eta^2N^2 - 8p\eta^2N + 2p\eta^2}{2p}, \tag{B.5}$$

$$b_1 = \frac{3d\eta - 4\eta N^2 p + 2\eta N^3 p - 7d\eta N + 2\eta Np + 5d\eta N^2 - d\eta N^3}{2p}, \tag{B.6}$$

$$b_2 = -\frac{3d + 2p - 4dN - 4\eta ap - 2Np + dN^2 - 4\eta N^2 p + 8\eta Np}{2p}, \tag{B.7}$$

$$b_3 = \frac{3d - dN + 2Np}{2p}. \tag{B.8}$$

References

[1] Li K, Bao B, Ma J, Chen M and Bao H (2022). Synchronization transitions in a discrete memristor-coupled bi-neuron model, Chaos, Solitons & Fractals, 165, 112861.

[2] Yan X, Li Z and Li C (2024). Dynamics and synchronization in a memristor-coupled discrete heterogeneous neuron network considering noise, Chinese Physics B, 33(2), 028705.

[3] Ma, Tao and Mou, Jun and Al-Barakati, Abdullah A and Jahanshahi, Hadi and Miao, Miao, Hidden dynamics of memristor-coupled neurons with multi-stability and multi-transient hyperchaotic behavior, Physica Scripta, 2023, vol. 98, pp. 105202.

[4] Ma, Minglin and Lu, Yaping and Li, Zhijun and Sun, Yichuang and Wang, Chunhua, Multistability and phase synchronization of Rulkov neurons coupled with a locally active discrete memristor, Fractal and Fractional, 2023, vol. 7(1), pp. 82.

[5] Vivekanandhan, Gayathri and Abdolmohammadi, Hamid Reza and Natiq, Hayder and Rajagopal, Karthikeyan and Jafari, Sajad and Namazi, Hamidreza, Dynamic analysis of the discrete fractional-order Rulkov neuron map, Mathematical Biosciences and Engineering, 2023, vol. 20(3), pp. 4760–4781.

[6] Goodrich, Christopher and Peterson, Allan C, Discrete fractional calculus, Springer, Springer, Cham, 2015, ISBN:978-3-319-09674-9.

[7] Sun, Huijing and Cao, Hongjun, Complete synchronization of coupled Rulkov neuron networks, Nonlinear Dynamics, 2016, vol. 84(4), pp. 2423-2434.

[8] Rulkov, Nikolai F, Modeling of spiking-bursting neural behavior using two-dimensional map, Physical Review E, 2002, vol. 65(4), pp. 041922.

[9] Du, Chuanhong and Liu, Licai and Zhang, Zhengping and Yu, Shixing, A coupling method of double memristors and analysis of extreme transient behavior, Nonlinear Dynamics, 2021, vol. 104(1), pp. 765–787.

[10] Wang, Caixia and Cao, Hongjun, Stability and chaos of Rulkov map-based neuron network with electrical synapse, Communications in Nonlinear Science and Numerical Simulation, 2015, vol. 20(2), pp. 536–545.

[11] Amirian, Mohammad M and Irwin, Andrew J and Finkel, Zoe V, Extending the Monod model of microbial growth with memory, Frontiers in Marine Science, 2022, vol. 9, pp. 963734.
[12] Khalighi, Moein and Sommeria-Klein, Guilhem and Gonze, Didier and Faust, Karoline and Lahti, Leo, Quantifying the impact of ecological memory on the dynamics of interacting communities, PLoS computational biology, 2022, vol. 18(6), pp. e1009396.
[13] Khalighi, Moein and Eftekhari, Leila and Hosseinpour, Soleiman and Lahti, Leo, Three-species Lotka-Volterra model with respect to Caputo and Caputo-Fabrizio fractional operators, Symmetry, 2021, vol. 13(3), pp. 368.
[14] Kaslik, Eva and Rădulescu, Ileana Rodica, Dynamics of complex-valued fractional-order neural networks, Neural Networks, 2017, vol. 89, pp. 39-49.
[15] Eftekhari, Leila and Amirian, Mohammad M, Stability analysis of fractional order memristor synapse-coupled hopfield neural network with ring structure, Cognitive Neurodynamics, 2023, vol. 17(4), pp. 1045-1059.
[16] Kaslik, Eva and Sivasundaram, Seenith, Dynamics of fractional-order neural networks, The 2011 International Joint Conference on Neural Networks, 2011, pp. 611–618.
[17] Suwan, Iyad, Mohammed Abdo, Thabet Abdeljawad, Mohammed Mater, Abdellatif Boutiara, and Mohammed Almalahi, Existence theorems for Ψ-fractional hybrid systems with periodic boundary conditions, AIMS Mathematics, 2021, vol. 7(1), pp. 171–186.
[18] Redhwan, Saleh S., Sadikali L. Shaikh, and Mohammed S. Abdo, Implicit fractional differential equations with anti-periodic boundary conditions involving Caputo–Katugampola type, AIMS Mathematics, 2020, vol. 5(4), pp. 3714–3730.
[19] Abdo, Mohammed S., and Satish K. Panchal, Some new uniqueness results of solutions to nonlinear fractional integro-differential equations, Annals of Pure and Applied Mathematics, 2018, vol. 16(2), pp. 345–352.
[20] Sadek, Lakhlifa, and Ali Algefary, On quantum trigonometric fractional calculus, Alexandria Engineering Journal, 2025, vol. 120, pp. 371-377.
[21] Sadek, Lakhlifa, Said Chablaoui, Ahmed Toukmati, El Mostafa Sadek, and Abdellatif Ben Makhlouf, On the Observability and Controllability of Linear Fractional Quantum Control Systems. Mathematical Methods in the Applied Sciences, 2025.
[22] Ghasemi, M.; Raeissi, Z. M.; Foroutannia, A.; Mohammadian, M.; Shakeriaski, F., Dynamic Effects Analysis in Fractional Memristor-Based Rulkov Neuron Model, Biomimetics, 2024, vol. 9(9), pp. 543.
[23] Hioual, Amel and Oussaeif, Taki-Eddine and Ouannas, Adel and Grassi, Giuseppe and Batiha, Iqbal M and Momani, Shaher New results for the stability of fractional-order discrete-time neural networks, Alexandria Engineering Journal, 2022, vol. 61(12), pp. 10359–10369.
[24] A. O. Almatroud, Extreme multistability of a fractional-order discrete time neural network, Fractal and Fractional, 2021, vol. 5(4): 202.
[25] Edwards, John T and Ford, Neville J, Boundedness and stability of solutions to difference equations, Journal of Computational and Applied Mathematics, 2002, vol. 140(1–2), pp. 275–289.
[26] Atici, Ferhan M., and Paul Eloe, Discrete fractional calculus with the nabla operator, Electronic Journal of Qualitative Theory of Differential Equations, 2009, pp. 1–12.
[27] Weinberg, Seth H and Santamaria, Fidel, History dependent neuronal activity modeled with fractional order dynamics, Computational models of brain and behavior, 2017, pp. 531–548.
[28] Liu, Li Jun and Qin, Ying Hua, Dynamics of discrete memristor-based Rulkov neuron, IEEE Access, 2022, vol. 10, pp. 72051–72056.
[29] Lu, Yan-Mei and Wang, Chun-Hua and Deng, Quan-Li and Xu, Cong, The dynamics of a memristor-based Rulkov neuron with fractional-order difference, Chinese Physics B, 2022, vol. 31(6), pp. 060502.
[30] Mohan, J Jagan and Shobanadevi, N and Deekshitulu, GVSR, Stability of nonlinear nabla fractional difference equations using fixed point theorems, Italian Journal of Pure and Applied Mathematics, 2014, vol. 32, pp. 165–184.
[31] Jonnalagadda, Jagan Mohan, Solutions of fractional nabla difference equations—existence and uniqueness, Opuscula Mathematica, 2016, vol. 36(2), pp. 215–238.
[32] Mert, Raziye and Peterson, Allan and Abdeljawad, Thabet and Erbe, Lynn, Existence and uniqueness of solutions of nabla fractional difference equations, Dynamic Systems and Applications, 2019, vol. 28(1), pp. 183–194.
[33] Nechvátal, Luděk, On asymptotics of discrete Mittag-Leffler function, Mathematica Bohemica, 2014, vol. 139(4), pp. 667–675.

[34] Jonnalagadda, Jagan Mohan, Matrix Mittag-Leffler functions of fractional nabla calculus, Computational Methods for Differential Equations, 2018, vol. 6(2), pp. 128–140.
[35] Acar, Nihan and Atıcı, Ferhan M, Exponential functions of discrete fractional calculus, Applicable Analysis and Discrete Mathematics, 2013, vol. 7(2), pp. 343–353.
[36] Cermák, Jan and Nechvátal, Luděk, On a problem of linearized stability for fractional difference equations, Nonlinear Dynamics, 2021, vol. 104(2), pp. 1253–1267.